Master *Radiation and its Effects on MicroElectronics and Photonics Technologies* (RADMEP)

APPLICATION OF HYBRID III-V ON SILICON LASERS TO NEAR-INFRARED SPECTROSCOPY

Master Thesis Report

Presented by

Meetsinh Thakor

and defended at

University Jean Monnet

09th September 2024

Academic Supervisor: Prof. Emmanuel MARIN

Host Supervisor: Dr. Jon Kjellman

Host Co-Supervisor: Dr. Liwang Liu

Jury Committee: Prof. Arto Javanainen, University of Jyväskylä

Prof. Paul Leroux, KU Leuven, Geel campus

Prof. Sylvain Girard, Université Jean Monnet

Prof. Frédéric Saigné, University of Montpellier

APPLICATION OF HYBRID III-V ON SILICON LASERS TO NEAR-INFRARED SPECTROSCOPY

Master Thesis Report

Presented by

Meetsinh Thakor

and defended at

University Jean Monnet

Master Radiation and its Effects on MicroElectronics and Photonics Technologies (RADMEP)

September 2024

Abstract

Silicon photonics (SiPh) is a rapidly evolving technology that takes advantage of silicon as an optical medium to create highly integrated and scalable photonic circuits for a wide range of applications. A variety of optical functions have been successfully implemented on this platform, leading to the development of complex and powerful Photonics Integrated Circuits (PICs). However, the integration of laser sources is still not fully developed, which hampers any further cost reduction for silicon photonic systems-on-chip and limits the expansion of this platform to more diverse applications. Making non-invasive continuous glucose monitoring (CGM) devices has been quite popular from the last decade but still haven't developed a device which is highly accurate, cheap and has a longer life span. This thesis is part of a big project for aiming a cheap CGM and gas sensing device based on photoacoustic spectroscopy (PAS). Here, we discuss a promising technology of making an on-chip laser source via the micro-transfer-printing (μTP) technique, which is currently in its earlier phase for adding III-V-based material on passive Si wafers. This on-chip laser source was designed under the internal development project of IMEC, and the fabrication of a 200 mm PIC wafer was done under IMEC's cleanroom facility and μTP was done in Ghent.

The thesis aimed to characterize the tunable lasers and their maximum modulation capability. Each laser die chip has multiple laser sources (called bank of lasers) and gives combined edge output in the range of 1400nm to 1700nm. The purpose of these lasers is to be used for PAS experiments and aim towards taking PAS out from the laboratory to real-life applications via making compact sensing devices for commercial uses. These laser sources are in the telecom band and have initial uses for detecting gas and glucose sensing. The project design has included many lasers for sensing purposes, we only see here two laser designs separated based on their waveguide material, an amorphous silicon (a-Si) based, and a second Silicon-nitride (SiN) based. This thesis includes understanding tunable on-chip lasers, as well as Vernier rings, phase shifters and Sagnac loop mirrors. The procedure includes cold cavity measurement and analysis of wafers which showed the second and third cavities are best for the narrowest output laser line width, the PCB designs task for each type of laser source which supports edge coupling laser output, further in chip processing and packaging the chip dicing, removing photoresistor, microscopic analysis of chips, electrical characterization of laser and wire bonding. For the laser characterization, discussing the experiment setup design, the result of nearly 70 nm tunning via both ranges of single laser source, and laser modulation was also allowed to sine and square wave for limit in several KHz.

Acknowledgement

I want to express my heartfelt gratitude and acknowledge the number of people who were always supportive and encouraging during my thesis. First, and foremost to my supervisor Dr Jon Kjellman who always motivates me to try new approaches and ideas. I can't imagine finishing this thesis without continuous assistance and support in each step by my co-supervisor Dr. Liwang Liu. I am very grateful for Joost Brouckaert's insightful comments and thorough analysis of my thesis work which has encouraged me to explore my research from diverse angles. Beyond my supervisors, Tangla David has provided me guidance through numerous discussions and meetings which has helped me a lot in this project.

I am also appreciative of IMEC for this internship opportunity which allowed me to join their remarkable team. IMEC provided access to essential research facilities, and their generous support helped me carry out my research work with cutting-edge lab facilities.

I would like to express my deepest gratitude to my academic supervisor, Prof. Emmanuel Marin, for his insightful feedback and unwavering support throughout my academic journey. I am also sincerely thankful to Prof. Sylvain Girard, Prof. Paul Leroux, and Prof. Arto Javanainen for their constant encouragement and guidance. Additionally, I extend my appreciation to all the faculty members and coordinators from the collaborating universities involved in the RADMEP program. Lastly, I am profoundly grateful to the European Commission for granting me the opportunity to be part of this exceptional master's program through the esteemed Erasmus Mundus Scholarship.

To my fellow friends and colleagues: thank you for the stimulating discussions and the experiences we have shared over the past two years. Special thanks to Tarique Hasan, Abhishek Padhy, Yogesh Bhosale, Afrina Hasan and Aditya Raj for always being there for any kind of help and support.

Lastly, I owe immense gratitude to my family for their unwavering mental support that sustained me throughout the thesis and beyond.

Table of Contents

List of Abbreviations

SiPh	Silicon Photonics
SOI	Silicon on Insulator
PIC	Photonics Integrated Circuits
NIR	Near-Infrared
PA	Photoacoustic
PAS	Photoacoustic Spectroscopy
μTP	Micro-Transfer Printing
SOA	Semiconductor Optical Amplifier
PCB	Printed Circuit Board
InP	Indium-Phosphate
MRRs	Micro-Ring Resonators
QCL	Quantum Cascade Laser
DFB	Distributed Feedback
a-Si	Amorphous Silicon
SiN	Silicon Nitride
GC	Grating Coupler
EC	Edge Coupler
FSR	Free Spectral Range
VR	Vernier Ring
PS	Phase Shifter
MMI	Multimode Interferometer
CW	Continuous Wave
MZI	Mach-Zehnder Interferometer
OSA	Optical Spectrum Analyzer
TEC	Temperature Controller
MZI	Mach-Zehnder Interferometer
PD	Photodetector
VCSEL	Vertical Cavity Surface Emitting Laser
ECL	External Cavity Laser
SMU	Source Measurement Unit
MHz	Mega Hertz
LED	Light Emitting Diode

List of Figures

1. Introduction

Integrated photonics has come a long way in the last 20 years, mainly because of its innovative integration platform. In its earlier time, to form an optical system the passive & active components were combined on a chip, but it was only used with III-V-based materials on the original substrate. Reducing propagation loss is a key component in the growth of integrated photonics and comparing SOI waveguides to III-V waveguides, the SOI has much-reduced propagation losses. The Significant development in Silicon photonics (SiPh) is driven by this lower loss, which improves the performance of coherent light sources and passive structures. [1] The range of applications for Si-based PICs has surpassed data communications and now includes sensing technologies like biosensors and automotive LiDAR, as well as emerging technologies like integrated quantum technologies, optical computing, and neuromorphic photonics and currently high demand for making on-chip spectroscopy devices. [2] Optical spectroscopy is an essential tool in physics, environmental sciences, chemistry, and biology for identifying a broad range of atoms and molecules.

In contrast to many other sensor types, spectroscopic approaches benefit from their selectivity, which is based not only on the chemical attraction of a molecule to a functionalized surface but rather on the distinct "fingerprint" of the spectrum. [3] The Laser-based spectroscopic techniques have shown to be very selective and sensitive at the same time, making them particularly appealing for trace gas monitoring and biosensing applications. Since a laser can only probe a single absorption line of the material to be studied, interference signals from other species may be avoided, allowing for excellent selectivity. This is made possible by the monochromaticity of laser sources and modulation in laser is also used in some of the spectroscopy methods. [4] Modulation techniques like photoacoustic spectroscopy (PAS), frequency modulation spectroscopy (FMS), and wavelength modulation spectroscopy (WMS) are used to achieve a high sensitivity.

PAS stands out among these methods because of its ease of use, great sensitivity, and wide dynamic range. A sample will absorb light at a certain wavelength, and the excited molecules will then relax to the ground state either via non-radiative mechanisms or by emitting photons. The non-radiative method on the sample experiences localized heating, which raises the local pressure. By the modulation intensity of the incident light being varied, the sample's thermal energy generation will also be varied accordingly, and a pressure wave that becomes, a sound wave will be generated at the same frequency as the incident light modulation. The PA cell signal may be strengthened with modulation frequency setting to one of the sample cell's acoustic resonances. [5] The main benefit of this method is it's a zero-background technique. Instead of looking dip in the transmission of absorption spectroscopy, The PAS signals are generated only when there is absorption, the sound waves it produces can be picked up by piezoelectric devices or a commercial hearing microphone. Further, this signal is analyzed with a modulated reference signal using a lock-in amplifier.

Figure 1 illustrates the concept of PAS. Given that the PAS technique relies on absorbed energy, mid-infrared gas lasers have been utilized for its development. These lasers can generate several watts of optical power within the spectral range where many molecules exhibit their strongest fundamental vibrational transitions. This makes them ideal for creating highly sensitive photoacoustic systems, capable of detecting concentrations in the parts-per-billion (ppb) range.

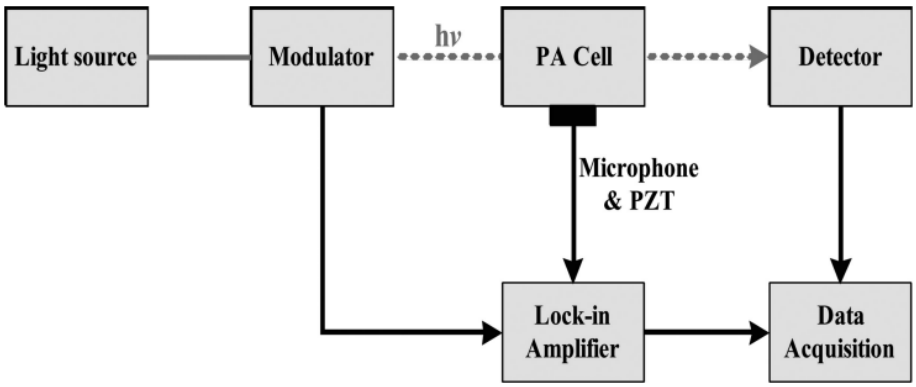

Figure 1: Illustration of the concept of Photoacoustic spectroscopy [12]

However, many applications do not need such high sensitivities, as well as making laser sources in those ranges is quite expensive. So currently, in these kinds of applications, distributed-feedback (DFB) laser diodes, III-V on silicon-based lasers, are operating in the near-infrared (especially telecom band) and are quite interesting. These semiconductor light sources have a long lifespan, are incredibly small, and operate at room temperature. [4] The laser sources that have the strongest absorption peaks are in the mid-infrared (MIR) 3-5 μm ranges but at the same time, they are expensive laser sources. The laser sources in the telecom band are widely used in 1.35–1.65 μm wavelength range and are cheaper than MIR sources. Many molecules have one or more absorption peaks which is also in the telecom range. Some of the molecules of interest (CO_2, NH_3, CH_4, C_2H_2, NO, H_2O, etc) are shown in *Figure 2* which shows the absorption cross-section bands versus the peak absorption wavelength plot from the HITRAN database. [6] HITRAN is an online website-based database for gas absorption peaks and absorption cross sections that tell the absorption strength of lines.

For the NIR sources, the optical power of laser diodes is much lower than that of mid-infrared gas lasers (compare several watts versus tens of milliwatts), well-designed PA systems based on laser diodes can potentially detect many species of interest at ppm or sub-ppm limits. Another important benefit of III-V on Si lasers is their compatibility with common optical fibers used in telecommunications. Given that the normal DFB laser tuning range of a is just a few nanometers, but the gap between the absorption bands of distinct species is typically considerably larger, it is usually necessary to employ multiple lasers in order to monitor many species simultaneously with a single instrument. [4] As a result, one laser is often needed for each substance. Also, the optical fiber has a low price and high coupling in the NIR range. Using an on-chip laser source and fibers reduces the dimension of the system as well as makes it more compact than bulky elements.

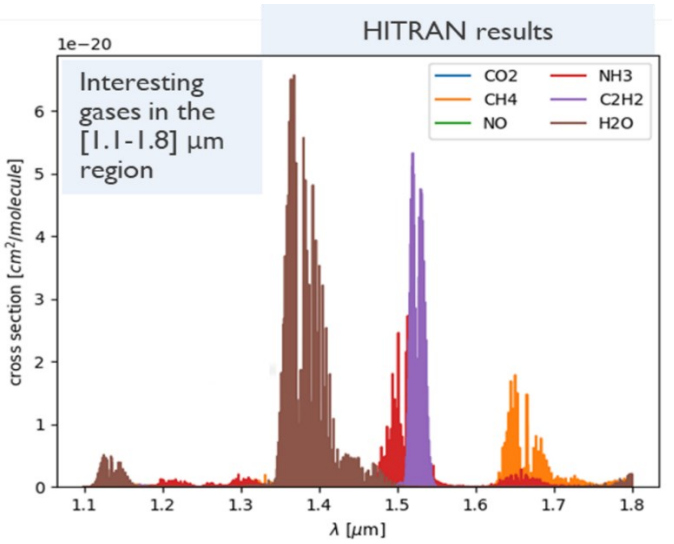

Figure 2: Plot of absorption cross-section vs wavelength in the NIR range of gases from the HITRAN database [6]

The absorption wavelength shown in the plot is from 1.1 to 1.8 µm in the NIR region for the gases. Out of all the gases, H_2O has a vast absorption band shown as in brown. While the weak absorption of the narrowest CO2 peak in blue is hidden close to the 1.4 µm.

A lack of on-chip light sources continues to be a major issue with silicon photonics technology. Because of indirect bandgap, silicon is unsuitable for laser operation or even for efficient light production. Consequently, a great deal of research has been done in the last ten years in the field of hybrid III-V-on-silicon integration, which involves the integration of III-V lasers on passively SOI PICs. [7] Creating highly reliable, stable, electrically pumped light sources on silicon is still difficult. There are several articles were published in a tuning range of around 100-120nm via two laser sources on a single chip. [26] The IMEC internal project was aimed at developing large tunable laser sources in NIR for PAS application. In the project, there are many different types of banks of lasers for a large range of 1400nm to 1700nm on a single chip. This thesis project is part of an effort to address this issue and create a large-scale tunability, modulation-capable, high-power on-chip laser source exploration for PAS applications. The combination of prefabricated III-V-based InP materials as diode coupons to print on the PIC offers a workable way to construct laser sources for SiPh applications. [8] With the availability of ultra-compact as well as photonics high-performance components like low-loss waveguides, with high quality factor micro-ring resonator (MRR), on-chip low-loss beam splitter and combiner, and widely tunable filters on the silicon photonics platform, hybrid III-V on silicon advances are trying to create advancement in laser sources for sensing applications. [8] The process of µTP can be used to integrate the active device into the passive PICs. This procedure allows for hybrid integration at the back end of technology by selecting and positioning suspended source coupons onto a host target [9].

The integrated on-chip tunable lasers shall benefit PAS in many ways including the Miniaturization which allows the compact and easy mobility of PAS systems. Tunability is very important which quickly sweeps across several wavelengths and allows detection of multispecies. The on-chip laser also consumes less power than the large laser components and similarly improves stability in terms of environmental perturbations and thermal management. The improved signal-to-noise ratio for PAS also has improved the sensitivity. The multiple lasers on a single chip enable parallel

measurements in terms of scalability. Last but not least the cost-effectiveness in terms of mass production of laser sources can reduce significant cost of the overall system because this is potentially a CMOS foundry compatible process that could be run in the same fabs making the low-cost electronics devices we are using every day. Together, these advantages make photoacoustic spectroscopy systems with integrated laser diodes more adaptable, sensitive, and useful for a variety of uses, including medical diagnostics and environmental monitoring.

1.1 Motivation of the Thesis

There is a high interest in developing a system that can detect several species with a single device that is compact, cheap, and easy to use. IMEC is well known for its advancement in research and future technologies. The photonics integrated circuits and systems (PICS) group at IMEC currently working on making a very cheap, large tunability, and modulation on-chip laser sources-based device in the telecom band for photoacoustic-based sensors. This internal project at IMEC has started to develop large tunability (around 300nm), modulation capability for PAS, stable, very compact, and very cheap (a few euros) laser sources for photoacoustic spectroscopy. As discussed before several gases have absorption peaks in NIR and one of the glucose absorption peaks in the same region. So, a high demand and market exists for a developing non-invasive continuous glucose monitoring device. The end goal is to make commercial devices that can be used widely. Reaching there has a long journey ahead; this thesis is part of a big project. The motivation behind making affordable photoacoustic devices for commercial use is that most PAS experiments are still limited to labs with bulky devices. My thesis is a part of this project, and my work is on the characterization of on-chip laser sources that were designed and fabricated at IMEC. To reach the goal of the thesis project the following necessary tasks were performed:

- Analysis of passive cavity performance (called Cold cavity measurement) of the fabricated wafer, this is a very helpful step before adding a semiconductor optical amplifier (SOA) InP (III-V material) based light source to the cavity.

- Based on the different types of lasers structures the design of PCB is a crucial step. Using the electronic functionality of on-chip laser sources induvial PCB design requires externally controlling them.

- To make an on-chip laser source on silicon, a micro-transfer printing method was used for it, and was done in collaboration with Ghent University to print SOA on the cavity.

- Chip Processing: This includes dicing laser chips, removing photoresistors, utilizing electronic characterization (I-V Measurements), and chip packaging.

- Experimental setup design for laser characterization: including building setup and configuring electrical devices, optical fiber alignment, and necessary mechanical components design, etc.

- The laser characterization includes maximum laser output power, optimizing maximum tunability, modulation, stability, noise, etc.

1.2 Outline of Thesis

For the thesis structure of the first chapter, we discussed the importance of PAS, its use in NIR sensing, and the motivation for this project. Chapter 2 focuses on the background information needed for the project including in detail PA spectroscopy and the important factors for PAS. Further, in a chapter, we will discuss the currently available sources for PAS and their advantages and disadvantages. Lastly, this chapter will talk in detail about the micro-transfer printing technique for III-V-based material printed on passive laser design.

Chapter 3, talks about the project design, introduces the tunable laser sources used for this project, and some functionalities of these laser devices. Further, we discussed the PCB design for these lasers.

In Chapter 4, the characterization of lasers discussed in detail the process for chip cleaning and other processing to the chip packaging, including cold cavity analysis, electrical characterization of devices, experimental design and setup preparation, and test results of the laser. Chapter 5 discussed the conclusion and potential future works in this project with included a bibliography and appendixes.

2. Background

This section discusses the history, working principles, and the key components of Photoacoustic spectroscopy (PAS), including light sources available for the PAS in several types and wavelength ranges. It also covers the current approach on III-V based on Si laser using the micro-transfer printing (μTP) technique and its comparison with current technology for on-chip laser sources.

2.1 Photoacoustic Spectroscopy (PAS)

Photoacoustic spectroscopy (PAS) traces its origins to 1880 when Alexander Graham Bell discovered the photoacoustic effect. [10] Bell found that sound could be generated when a sunbeam was sharply interrupted and focused onto narrow diaphragms using a spinning slotted disc. This occurs because the absorbed solar energy is converted into kinetic energy, leading to localized heating and the creation of a pressure wave, or sound. PAS can measure the photoacoustic spectrum of a sample by detecting sound pressure across various wavelengths and is effective for analyzing solids, liquids, and gases due to its sensitivity to sample absorption rather than scattering losses. Despite its initial promise, research into the PA effect declined for several decades due to the lack of sensitive microphones and a clear quantitative understanding.

Interest in PAS was revived with the development of lasers, which provided the high spectral brightness needed for more precise measurements. In 1968, a continuous-wave CO2 laser in a PAS system to measure the absorption spectra of carbon dioxide molecules, demonstrating the technique's potential for detecting trace air pollutants. Their work highlighted the advantages of using lasers and phase-sensitive lock-in techniques to amplify the acoustic signal, making PAS a valuable tool for trace gas detection. [10] Since then, significant advancements in light sources, modulators, and PA signal transducers—particularly with the development of semiconductor diode lasers—have expanded PAS's applications to fields like industrial process control, chemical analysis, medical diagnostics, atmospheric monitoring, and life sciences. [12].

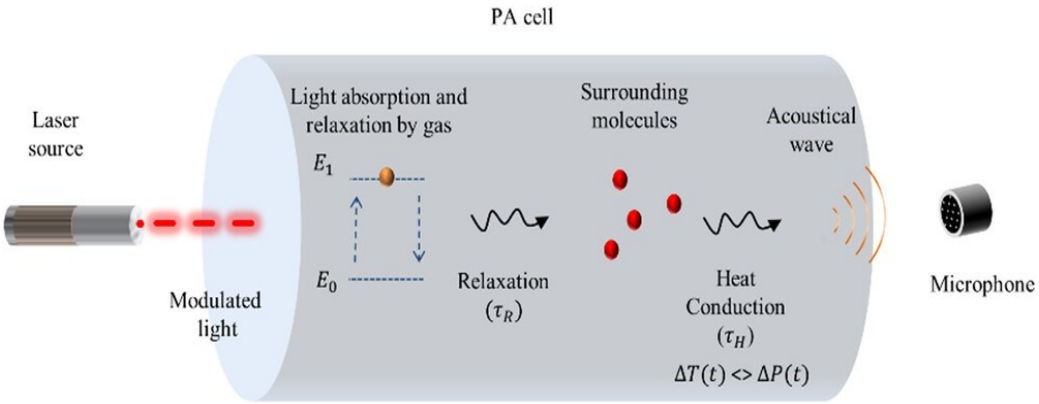

Figure 3: PAS mechanism based on laser source, light absorption, relaxation, heat-conduction and acoustics wave generation [13]

The PAS approach offers the ability to provide trace gas analysis that is comparatively inexpensive, small, durable, very selective, extremely sensitive, and has a huge dynamic range. *Figure 3* presents a basic diagram of the PAS mechanism.

The excitation light source, for example, an LED, different types of lasers, or simply a white light source. An acoustic cell is filled with a gas that absorbs the optical power at the excitation wavelength. This results in the molecules experiencing an increase in the energy. Afterwards, the molecule relaxation energy goes into a nonradiative state of translational or kinetic energy, through inelastic collisions. This procedure takes place in the interval known as the relaxation period τ_R. As a result, the local temperature T rises, causing the local pressure P to rise. After that, in a reaction time of τ_H, the heat energy moves to the cell walls. When the amplitude of the excitation light is modulated, an acoustic wave is produced, causing changes in pressure over time. [13] The acoustic wave can then be detected by a microphone, through propagation inside the PA cell. The sensitivity of the PA sensors can be enhanced by operating at the resonance frequency of the PA cell, which is mostly determined by its shape.

The laser source and its modulation are crucial to the PAS, because the intensity of the source beam is directly proportional to the PA signal, indicating the significance of light source modulation. When it comes to the laser, detecting the second harmonic signal and using wavelength modulation are more effective. When wavelength modulation is used, the PA signal is not affected by the losses introduced by the walls and windows, but rather by wavelength-dependent losses like the gas absorption lines [13]. In contrast to traditional sinusoidal modulation, quasi-square and triangle-shaped waves improve the photoacoustic signal in several ways.

In pulsed or modulated light radiation absorption at a wavelength that aligns with an absorption characteristic of molecules of interest. The absorbed electromagnetic energy is transformed in periodic local heating of molecules at a modulation frequency during the nonradiative collisional relaxation processes. [12] Within the PA cell, a standing pressure wave is created that may be identified using phase-sensitive lock-in methods, piezo transducers, commercial microphones, or other pressure detectors. The equation of the PA signal, S, is expressed as follows:

$$S = S_m \, P \, C_{cell} \, N_{tot} \, C_m \, \sigma \tag{1}$$

Here, the measured sensitivity of the microphone S_m in millivolts per Pascal, Optical power is P in watts, C_{cell}, is the response constant of the PA cell, measured in Pascal per inverse centimeter per watt, N_{tot} is the total number density of molecules and has a unit of molecule/cm^3, and the concentration coefficients C_m and σ for the absorption cross-section of analytes. As per the equation, both incoming strength of the light source and concentration of molecules is proportional to the PA signal.

Based on the light source type it may restrict the accessible excitation soundwave frequencies and the modulation may take several forms. Thermal light sources (e.g. incandescent lamps) are currently restricted to frequencies of about several Hz when depending on the driving current of the light source for intensity modulation [14]. A chopper may be used to produce higher modulation frequencies utilizing heat sources. However, the driving current of diode lasers and light-emitting diodes (LEDs) may be adjusted to vary the light's intensity. In principle, frequencies as high as several MHz are possible. Wavelength modulation is an additional approach for producing a photoacoustic signal when employing single-mode lasers [15]. However, for the system to respond the modulation frequency needs to be lower than the inverse of the molecular relaxation period ($1/\tau_R$).

Since then, researchers have concentrated on PAS analysis and achieved notable advancements, including the invention of procedures, the development of theoretical ideas, and innovative apparatus. [12],[16] After having foundational principles and applications of PAS it is necessary to talk about the crucial role of light sources in this

technique. As discussed earlier, the choice of a light source affects the sensitivity and determines the suitability of various samples and molecules. The development of a high extinction ratio, extensively tunable, and highly modulated on-chip laser source in the telecom band was the main goal of this thesis project.

2.2 Light Sources for PAS

The choice of the light source is influenced by different factors. Its primary requirement is to supply a wavelength that is appropriate for the analyte of interest to be detected. For a sensitive examination of the analytes, generally, a narrowband light source operating in the infrared (IR) or near-IR (NIR) spectrum is needed. Databases and the literature often include the absorption spectra of most molecules. To match one of the absorption bands of the analytes, the wavelength needs to be precisely adjusted [16]. Another additional criteria for considering the light source is whether an appropriate device is available that can supply the selected wavelength and the necessary small line width. Also, to achieve an appropriate sensitivity, which can vary depending on the application and the sample, a particular optical emission power is required. So, for detection of multiple samples in different wavelengths, large tunability from a single source is important [16]. Moreover, the working of the light source must be in a pulsed or modulated way. Even though it seems like a small need, not all light sources can be directly manipulated. A variety of lasers (CO_2, QCL, etc), especially high-output power laser sources are difficult to operate steadily because of modulation as it causes thermal instability. This part talks about some of the available light sources for the PAS and an innovative approach with a tunable on-chip laser source.

The light source to a PAS is very crucial, and therefore it should ideally have a compact footprint, a large tuning range, a narrow spectrum resolution, a tiny linewidth, and a high cost-efficiency (more applicable and inexpensive). Currently, there are many available light sources which include QCL, DFB laser, LED, MEMS, double comb, III-V diode laser and many more. Out of which, we have discussed a few of them here and compared their pros and cons.

Quantum Cascade Laser (QCL): was firstly demonstrated in 1994 [17]. The basis of the QCL is formed by the multiple quantum wells organized in a periodic arrangement. Photon emission occurs during intersubband or intraband transitions involving discrete electronic states introduced by each quantum well within the band structure. The distance from the states, and consequently, the thickness of layers can controlled by the emission wavelength. Then electron emits a photon, undergoes intra-band tunnelling to the next quantum well, and continues this process. One electron can emit many photons, increasing the laser's efficiency. Over the past ten years, successful attempts have been made to raise QCL's overall efficiency for both continuous and pulsed operations. A wide spectrum range of 5.9 to 10.9 μm was covered by stacking different wavelength quantum cascade stages, using a single device with a peak output of around 50 mW. However, the primary drawback of QCLs is their high cost, coupled with a significant threshold current, leading to high power consumption.

Furthermore, QCL performance is restricted to wavelengths larger than 4 μm. Inter-band cascade lasers (ICLs), like QCLs, rely on cascading multiple layers and involve inter-band transitions—transitions between the valence and conduction bands—similar to those in laser diodes. [13]. Following photon emission, electrons undergo inter-band tunneling from the valence band to the conduction band within one layer, and then continue this process to reach the next layer. ICLs enable tunable diode laser spectroscopy for absorption, paving the way for innovative applications in industrial gas sensing within the mid-infrared (MIR) region. The strongest absorption bands of several industrially significant trace gases are located in the 3 μm to 6 μm wavelength

range, which is currently covered by inter-band cascade lasers. Today, the continuous wave (CW) output powers of QCLs typically reach several milliwatts, with reports of exceeding 100 mW. Recent advancements in external cavity QCLs have extended the tuning range to ±5% of the central wavelength. In particular, the critical 3–4 μm range currently faces limitations in both tuning capabilities and wavelength coverage [19]. However, QCLs remain a highly promising source for gas sensing applications.

DFB lasers: A DFB (distributed feedback) Laser in its simplest configuration, the laser system achieves feedback through two mirrors that form a Fabry–Perot cavity. It typically has a broad bandwidth and can result in multimode lasing. To address this issue, a DFB laser incorporates a diffraction grating on top of the active layer, providing narrowband feedback and thereby reducing multimode operation. This technique works with QCL, ICL, and laser diodes. An alternative method, known as a vertical-cavity surface-emitting laser (VECSEL), can also be used that applies a multilayer Bragg reflector on top and to the bottom active layer from where the laser beam is going to be emitted vertically. [13] An external cavity is employed to achieve a broader tuning range by using the active medium of the laser in conjunction with a wavelength-selective element, such as a diffraction grating, to adjust the wavelength. By adjusting the temperature of the device, the DFB's wavelength may be adjusted within a certain range. And a larger tuning range may be reached, by arranging many DFBs in an array with a multimode interference coupler. It is possible to obtain the wavelengths between each component, by adjusting the overall temperature of the chip, however doing so results in a rather large power consumption.

MEMS-based tunable lasers: The Micro-Electro-Mechanical Systems (MEMS) is a technology used to create compact, widely tunable laser sources for PAS. The Key developments in MEMS include a moveable MEMS-based top mirror, and a tunable VCSEL offers an alternative method. Generally, VCSELs are used at wavelengths between 850 and 1330 nm. However, it is difficult to produce VCSELs at wavelengths of about 1550 nm [19]. Integration of VCSEL with MEMS mirrors can have a wide tuning range through mechanical adjustments of the cavity length. Mirror tuning rates can reach several kilohertz, but another approach involves using MEMS-based External Cavity Lasers (ECLs), which provide enhanced spectral purity and enable mode-hop-free tuning.

Another type of tunable laser is the external cavity laser with an integrated wavelength-selective filter. The wavelength filter is usually a diffraction grating, and can be adjusted by translating or rotating the retro-reflecting mirror. As the DFB array and VCSEL-based tunable lasers, have the same drawback which is mostly their incapability to be used for applications requiring fast wavelength switching [19]. There are external cavity III-V diode lasers that are readily available as well. They are compact, robust, and have great tuning properties, making them excellent sources. When run at ambient temperature, they give CW powers in several mW and small linewidths. The visible to around 2 μm are the available wavelengths and depending on the center wavelength, several tens of nm can be tuned [18].

III-V on Si Sources: In PICs, combine many optoelectronic processes into a single chip. Even though most optical functionalities have been successfully incorporated by engineers into silicon photonic circuits, because silicon's indirect band gap prevents efficient light generation, light emission is still difficult. This causes the requirement of light generation by employing the III-V semiconductor materials, usually in the form of district components. However, because of its limitations in terms of cost, space, and reliability, there is an increasing need to incorporate these lasers directly into silicon chips. Some of the primary approaches for the integration process including monolithic integration, flip-chip processing, die-to-wafer bonding, and micro-transfer printing are

being investigated [20]. Every technique has its special advantages and difficulties which concern accuracy, scalability, and manufacturing costs. On-chip lasers have demanding future market opportunities in PIC-based sensors, as they have a wide tunability, narrowest linewidth, modulation capability of laser sources, and possibly the development of on-chip acoustic sensors. For that, a cheap laser source is essential and based on current laser technologies, we need to find the best and cheapest way to make it for commercialized devices.

Micro-transfer printing uses van der Waals forces and adhesive or molecular bonding to secure lasers in place, in contrast to flip-chip technology, which employs metallic solder bumps. By placing the laser on top of silicon-waveguide structures, evanescent coupling—a less exact alignment than butt-coupling—allows light to "bleed" into the waveguide. The potential for faster throughput is demonstrated by the ability to transmit data to thousands of devices simultaneously, thanks to this increased tolerance. IMEC tested this method with promising results by affixing light sources to wafers containing SiPh waveguides and other components. Based on their prediction, the technology will be ready for production implementation within a few years.

In the next part we will discuss another possible and cheap technology that can be used for laser integration is discussed.

2.3 Micro-transfer printing (µTP) for III-V on Si Lasers

In 2004, the Roger group at the University of Illinois developed a technique called Micro-transfer printing (µTP) [21]. It is a recent integration technology using which micrometer-sized thin film materials and devices can be manipulated and transferred massively in parallel from the source to the target substrate with medium alignment accuracy (±0.5 µm for each coupon placement). Additionally, for a single printing cycle, it takes around 30 to 45 seconds, making it a relatively quick procedure. However, by prefabricating coupons or devices in a dense array of III-V wafers, the efficiency of III-V-based materials using µTP is greatly increased compared to the costly epitaxial growth. [22]

Using µTP the components can be pre-tested on their native substrates, before being integrated into a target Si PIC wafer, much like with the flip chip assembly. In theory the III-V substrate for the µTP method is possible to reuse, which can lead to additional cost reductions. Table 1 here enlists the pros and cons of different strategies. As compared to the epitaxial growth technology, if we look at µTP, it is quite new and currently in the research and development phase. But in the end, the technology with low cost, high efficiency, and high alignment accuracy will be widely used in the future for the development of laser sources using III-V-based material integration on silicon.

Technology	Integration density	Efficiency of III–V material use	Alignment accuracy	Throughput	Cost	Maturity
Flip-chip	Low	Medium	Medium	Low	High	Mature
Bonding	Medium	Medium	High	High	Medium	Mature
Epitaxial growth	High	Very high	High	High	Medium	R&D
μTP	High	High	Medium	High	Low	R&D

Table 1: Overview of Different Wafer-Level Heterogeneous Integration Methods for III-V-on-Silicon [25]

Among the four techniques mentioned in Table I, flip-chip, and μTP techniques are good for making hybrid multiple SOA-based laser sources on a chip. High-power SOAs are used in spectroscopy, LiDAR, optical communication, and other areas. Because of the low loss and efficacy of the SOAs, in the field of optical fiber communication, the 1550 nm band [23]. The SOAs are widely used as laser sources because they are smaller and less expensive than erbium-doped fiber amplifiers.

For creating SOAs, direct bandgap semiconductor materials are used. In these semiconductors, electron-hole recombination can occur without a change in momentum, meaning it does not require interaction with the crystal lattice. In a device like this, electrons and holes are introduced into different energy states, where the electrons inhabit the conduction band, and the holes occupy the valence band. It is feasible for semiconductors with a direct bandgap to experience a population inversion. [24] In these circumstances, when undertaking stimulated emission in the context of an electromagnetic wave, electrons from the conduction band recombine with the holes in the valence band.

Layer	Layer type	Material	Thickness [nm]	Doping level [cm^{-3}]	Dopant
26	Cap P	InP	100	$\approx 1 \times 10^{19}$	Zn
25	Contact P	GaInAs (lattice matched)	200	$\approx 2.5 \times 10^{19}$	Zn
24	Transition P	GaInAsP (λ_g = 1170 nm)	20	$\approx 6 \times 10^{18}$	Zn
23	Cladding P	InP	1000	$\approx 1 - 2 \times 10^{18}$	Zn
22	Cladding P	InP	500	$\approx 5 \times 10^{17}$	Zn
21	Etch stop	GaInAsP (λ_g = 1170 nm)	25	$\approx 5 \times 10^{17}$	Zn
20	Transition	$(Al_{0.9}Ga_{0.1})_{0.47}In_{0.53}As$	25		
19	SCH	$(Al_{0.7}Ga_{0.3})_{0.47}In_{0.53}As$	25		
8x6	Barrier	$(Al_{0.45}Ga_{0.65})_{0.51}In_{0.49}As$	10		
7x6	Well	$(Al_{0.25-0.20}Ga_{0.75-0.80})_{0.3}In_{0.7}As$	6		
6	Barrier	$(Al_{0.45}Ga_{0.65})_{0.51}In_{0.49}As$	10		
5	SCH	$(Al_{0.7}Ga_{0.3})_{0.47}In_{0.53}As$	25		
4	Transition	$(Al_{0.9}Ga_{0.1})_{0.47}In_{0.53}As$	25	1×10^{18}	Si
3	Cladding N	InP	200	2×10^{18}	Si
2	Sacrificial	GaInAs (lattice matched)	50	nid	
1	Sacrificial	AlInAs (lattice matched)	500	$\approx 1 \times 10^{18}$	Si
0	Buffer layer	InP	150	nid	

Table 2: The sample of III-V-based epitaxial layer stack of SOA with multi-quantum wells (MQW) variants to achieve light peak on 1500nm to 1550nm. [26]

Table 2 shows the SOA epitaxial stack consists of six QWs active regions sandwiched between the barrier layer, a 200 nm contact P layer with 20 nm transition layer P underneath, with a 1 μm+ 0.5 μm cladding of InP, with three 25 nm etch stop, transition and SCH layer, two 10 nm AlGaInAs transition layers with 6 nm well is separating two SCH layers, further cladding and sacrificial layers were present with laser buffer layer of 150nm. [27] based on these two stacks there are another two laser emissions around 1525 nm and 1575nm that can be made. A Silicon taper, which is the point between SOA and the waveguide, to get maximum coupling light from SOA to a waveguide. The taper is used to compensate for the coupling losses caused by the inherent misalignment due to the transfer printing [28]. The wide Silicon waveguide gradually narrows into a single-mode waveguide outside the III-V on Silicon SOA through an adiabatic taper.

Figure 4 illustrates the concept of μTP, enabling the close integration of multiple materials on a single chip, along with the integration sequence. These devices are lifted from the source wafer and transferred onto a new target substrate using an elastomeric polydimethylsiloxane (PDMS) stamp. PDMS is cast into a silicon master mold to create the stamp, resulting in post arrays with dimensions and pitch that precisely match the device arrays fabricated on the source wafer. As seen in *Figure 4*(a), the stamp is laminated on a clear wafer following its release from the Si master.

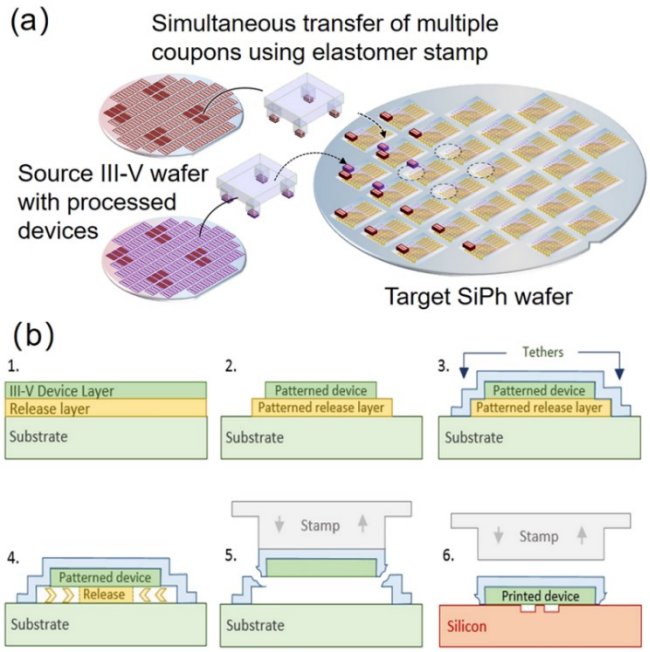

Figure 4: The concept of micro-transfer printing (a) Schematic of μTP-based integration on SiPh wafers to parallel manner and (b) prefabrication of III-V devices on their native substrate and the μTP integration sequence [25]

In the μTP technique, a prefabricated InP-based SOA is lifted from its original III-V source wafer using a PDMS stamp and then printed onto the target substrate. This substrate features recesses on its backside that align with the μm-wide Si waveguide. This method, which also does not require the processing and singulation of every single III-V chip and only modifies the SiPh process flow slightly, enables wafer-scale III-V integration and high throughput (significantly parallel) [26]. Patterned on the III-V source wafer, these devices include local apertures that provide access to the release layer. An encapsulating layer, typically a photoresist layer for III-V devices, protects the devices. The release layer remains beneath the devices to ensure precise alignment and registration of the III-V devices both during and after the release process. The PDMS stamp is swiftly pulled back from the original substrate after it has laminated the stamp onto the wafer, the device array is carefully positioned and transferred to target wafer by retracting the stamp. This process is depicted in steps 1-6 of *Figure 4*(b).

After successfully and manually finishing the μTP process, the further metallization step is followed to make it conductive. For that, mostly gold material is used.

3. III-V on Si laser Sources, their Functionalities, and PCB Design

As discussed earlier for the PAS experiment the most crucial thing is the laser source. From the multiple different laser sources designed in this project, two tunable laser sources and one DBR bank of lasers were mainly focused on this work which will be further discussed here. To characterize the on-chip laser source first we need to understand the laser design and the functionalities it offers. Here we will discuss two tunable lasers with slightly different designs and two different waveguide-based laser sources. Each laser output of the chip can give a combination of four different wavelengths through the edge coupling (EC). Further, we will discuss all the functionality and working principles of the components used in these lasers and for utilizing all the laser functionality the necessary PCB design will be discussed which is important to package those lasers for characterization.

The name of these lasers was given based on their waveguide material. The first tunable laser design is an Amorphous silicon (a-Si) based waveguide so-called "aSi laser" and the second laser design is based on the Silicon-Nitrite (Si_3N_4) base waveguide so-called "SiN laser". Here the two different waveguides were purposely used to get the best performance of the lasers. The main purpose of the two different designs is to find the best solution between these waveguides based on waveguide losses, coupling losses, the minimum power required to change the index of materials and the maximum operating power, etc. An aSi waveguide has larger losses than a SiN waveguide, but aSi is more temperature-sensitive than SiN. The material's thermo-optic coefficient sets this temperature sensitivity. So, for the same amount of tuning, the SiN waveguide consumes more power than the aSi waveguide.

In the project design, both device designs have their own three replicas with the only difference in the coupling gap between the waveguide and vernier rings. *Figure 5* shows one of the rings with a waveguide size of 1 µm and a coupling gap of 0.5 µm. The other three copies have coupling gap differences of 0.2 µm, 0.3 µm, and 0.4 µm.

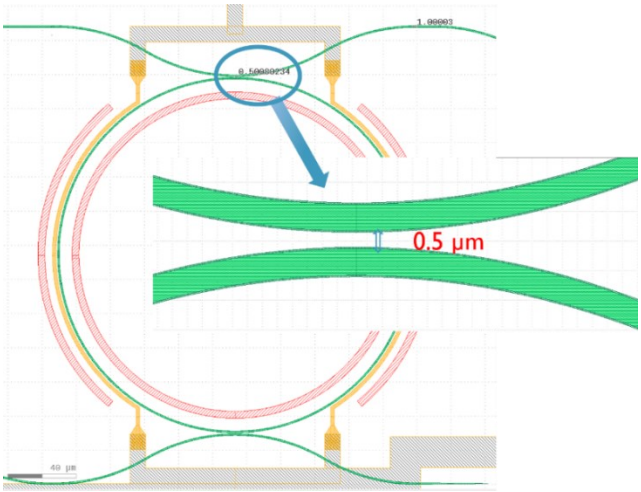

Figure 5: Coupling gap distance 0.5 µm between the ring and waveguide as from the design

The purpose of designing multiple devices with different gaps is to the find best laser output four which gives the narrowest line width of the output wavelength peak. Which is very important for the absorption peak of molecules. In conclusion, there are four

laser designs for aSi laser and four laser designs for SiN laser with only a change of coupling gap between the waveguide and vernier ring.

3.1 Tunable Amorphous silicon (a-Si) lasers

As one of the material phases of silicon, amorphous silicon (a-Si) has a disordered silicon network as opposed to crystalline silicon, which has ordered Si atoms grouped in a tetrahedral configuration. Differential electrical and optical properties were first investigated for broader applications, such as integrated photonics, but were initially created for microelectronics and solar cell applications. a-Si is deposited as a thin layer at comparatively low temperatures (20–400°C) on a substrate in integrated photonics. The material must be deposited at low temperatures in order to preserve its amorphous state otherwise, it will crystallize and create polycrystalline silicon. [29] A common method for fabricating microelectronics is PECVD for the deposition of a-Si.

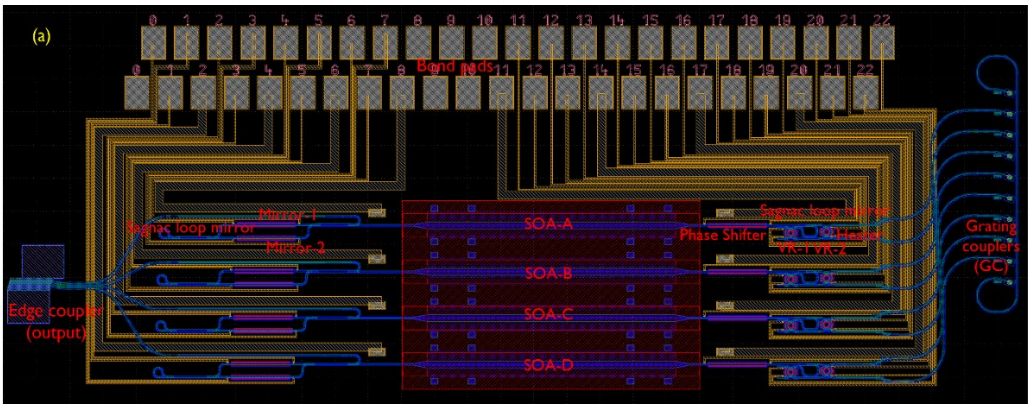

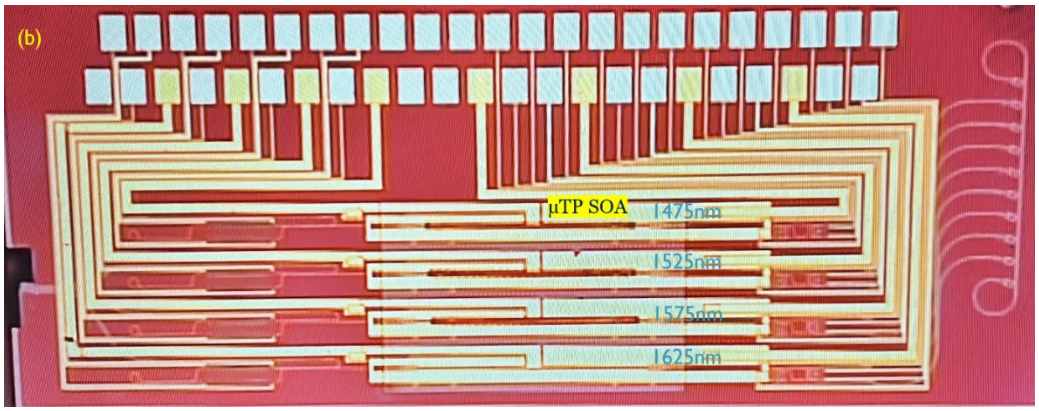

Figure 6: The aSi laser (a) Tunable aSi Laser design from K-layout, (b) Microscopic image of the fabricated and µTP on SOA for different wavelengths laser used for the experiment

Improved lithography and etching have led to a reduction in optical losses in Si waveguides, which are often caused by light scattering at rough surfaces. Losses in Si waveguides are currently far below 1 dB/cm. With the temperature of the waveguide higher than 200°C the propagation loss starts to increase exponentially. [30]

For this project, the aSi waveguide-based laser design is shown in *Figure 6*(a) it has four a-Si waveguide-based single chip die. In each chip, there are four SOA-based laser sources and output is combined from the edge side. Each laser has an individual cavity

for SOA, a thermo-optical phase shifter for fine-tuning the wavelength, Two thermally tuning vernier rings with slightly different sizes, and both sides tunable Sagnac loop mirrors with edge coupler (EC) and grating coupler (GC) on opposite sides for taking output. As discussed, four chips are separated based on the coupling distance between the waveguide and resonator rings, the four aSi lasers are named aSi_1, aSi_2, aSi_3, and aSi_4, based on their coupling distance are 0.2 μm, 0.3 μm, 0.4 μm, and 0.5 μm, respectively. As per design single chip has four identical lasers by doing μTP at SOA region with different peak wavelengths. In four laser cavities, each with a distinct gain peak wavelength is 1425nm, 1525nm, 1575nm, or 1675nm into a SOA, a widely tunable laser is created. As seen in *Figure 6*(b), it is a microscopic image of the laser after fabrication and SOA μTP in brown. For the laser output, the optimization of out-coupling mirror reflectivity is made possible by the tunable Sagnac loop mirror. Wavelength selection is made possible by the Vernier filter, which is formed by the tunable MRRs. For the thermo-optic heating Titanium nitride (TiN) based material was used. The wire and bond pads are made with Al and used for external connection with a wire bonding to the PCB pad by injecting electric power into those components.

The parameter used for the components is the following: the a-Si waveguide has a width of 0.5 μm. The chips' four waveguides are separated with isolation trenches and each waveguide will have laser sources. The designed diameters of the two rings were slightly different. The first ring with a diameter of 50 μm and the second ring has a diameter of 53 μm. As calculated FSR from the equation, which is 3.5 nm. The SOA length is 1.5 mm and consists of two adiabatic tapers which have a length of 145 μm with a beginning width of 2.5 μm and an ending width of 0.6 μm with these two tappers ensure the effective coupling between SOA and waveguide. The length of the 2x2 MMI coupler is around 190 μm. The area of the laser chip is (width x length) = (6000 μm x 2500 μm). The approximate length of the laser cavity can be around 2700 μm and the length of the TiN heater is 400 μm. Modern commercial micro-transfer printing technology can achieve alignment precision between the adiabatic taper and the SOA. The GC is used to couple single-mode fiber to the power meter and from the EC the optical spectrum was recorded. The number of modes supported in the cavity is very high and the FSR of the cavity calculated from the equation is 0.2nm (200 picometers). So, uniform modes inside the cavity can be considered.

3.2 Tunable Silicon nitride (SiN) lasers

silicon nitride (SiN) on an insulator is a potential new material framework that is transparent in the wavelength range of 400–5000 nm. In silicon nitride (Si_3N_4) waveguides, significantly lower losses can be attained due to a lower index contrast than silicon. Furthermore, SiN exhibits less thermal fluctuation than silicon due to its lower thermal coefficient which means to change the refractive index more power is needed than silicon. The advantages of the silicon-on-insulator waveguide platform also apply to silicon nitride circuits, as they might be produced in a CMOS fab. [31]

The tunable SiN laser design used for this project is shown in *Figure 7*(a), which has also the same components as those used in aSi laser design. The major change is waveguide material, which used less number of bond-pads and EC output is the opposite. Here it has also vernier rings, a Laser cavity for SOA, a phase shifter, a Sagnac loop mirror, GC, and EC. The TiN material is used as a heater, and it is closely placed on waveguides. All the heaters are externally connected with an Al tiny wire to the bond pads. These bond pads will be connected to the PCB pads. *Figure 7*(b) shows the microscopic image of the SiN laser die after the μTP.

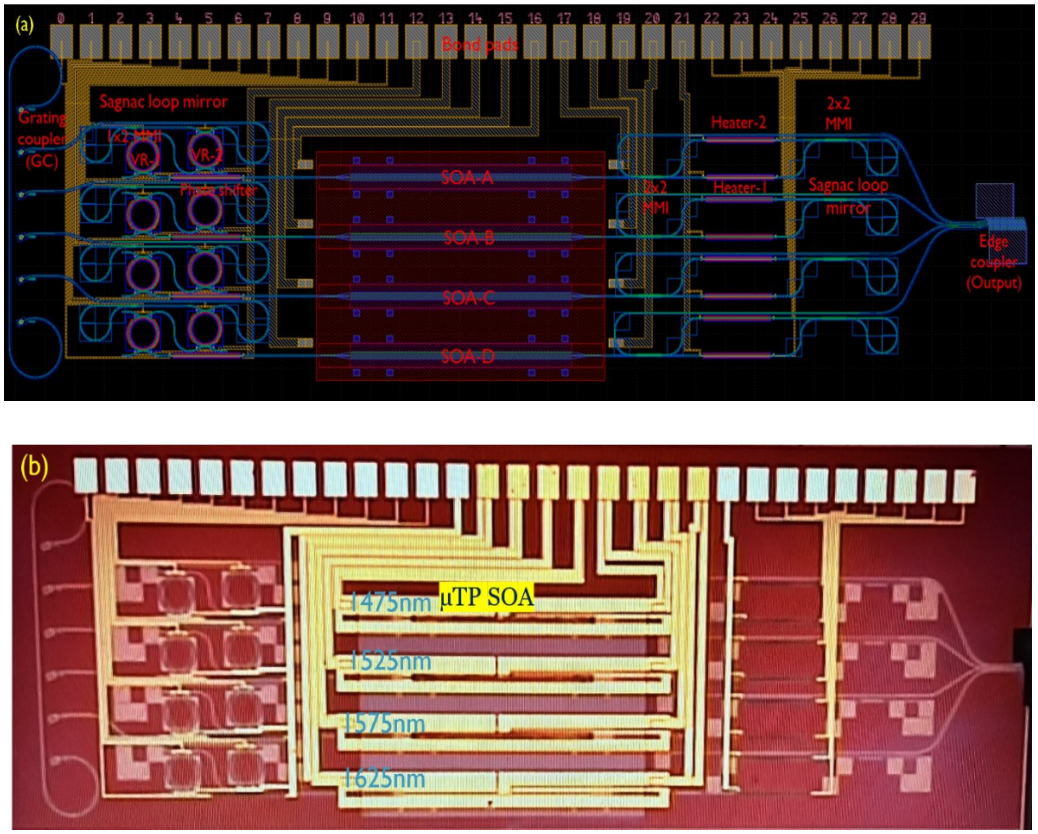

Figure 7: SiN laser (a) Tunable SiN Laser design from K-layout, (b) Microscopic image of the fabricated and µTP on SOA for different wavelengths laser used for the experiment

From the design SiN waveguide width is 0.9 µm. The chips' four waveguides are separated with isolation and each waveguide has SOA-based light sources whose peak wavelengths from one of 1425nm, 1525nm, 1575nm, or 1675nm. The designed diameters of the two rings are slightly different from each other. The first ring has a diameter of 200 µm and the second ring has a diameter of 207 µm. As from the FSR calculation, the FSR for the VR is 2 nm. Here the SOA length is 1.5 mm and the 2x2 MMI coupler length is around 153.6 µm. The area of the laser chip is (width x length) = (7000 µm x 2500 µm). The approximate cavity length is around 3200 µm and the same length of the heater with aSi design is 500 µm.

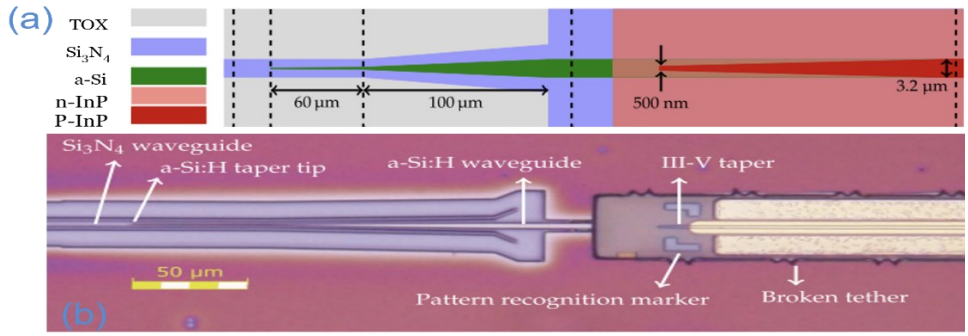

Figure 8: SiN taper (a) schematic layout of the two-step taper in SiN laser (b) optical microscope image of the µTP of III-V material on SOA [32]

The low refractive index of SiN prevents phase matching between the III-V mode and the SiN waveguide, which blocks coupling light from III-V to the SiN. So there is a need to add a taper which can connect to this waveguide. For the taper new intermediary aSi layer is added to fix this problem. So the light from III-V to the aSi layer which is further coupled to SiN waveguide. *Figure 8* shows the schematic of only one side of the SiN laser, the size and materials in a two-step taper are shown in *Figure 8*(a) and the microscopic image of the fabricated laser with the μTP of III-V material on SOA in *Figure 8*(b). [32] The III-V-based material of SOAs is 1.5 mm long and consists of two adiabatic tapers on both sides of the SOA. The other component like the GC is used to couple single-mode fiber in the power meter and the EC for the optical spectrum is recorded via OSA.

3.3 Design Printed Circuit Board (PCB) for Lasers

Because of its many functions, PCB is an essential component of modern electronics. The integrated photonics chips benefit most from heat dissipation, mechanical support, and stability. Furthermore, the device's compactness and miniaturization offer significant advantages in terms of space efficiency as well as a decrease in weight and size. Additionally, the automated assembly and simplicity of manufacture provide a long lifespan at a reasonable cost while maintaining consistency in quality.

For the a-Si and SiN laser sources, both lasers have a special number of bond pads, shapes, and sizes that make them induvial. For the PCB design, KiCad software version 8.1 was used. To get the final PCB first, it starts with the schematic drawing by creating the required number of pins and pads. For the aSi laser, it has a complex design, and it has a greater number of bond pads than the SiN laser design. In the schematic design, it is quite simple and the footprint is attached to the design. The footprint is a physical representation of the precise sizes, shapes and arrangement of the pads.

After the schematic drawing, the design was imported into the PCB editor. In the editor, where we can visualize our real PCB, the components were placed exactly at the distances required based on the laser design. The heatsink was designed for laser placement and pin-through holes were used in the heatsink design, for quick heat dissipation. While laser testing the chip will be placed on the heatsink. Based on the edge design laser source after properly arranging the bond pads and heatsink location still need to fix four M4-size screws. These four screws will allow PCB to fix it on the temperature control Chuck. After all the components are placed and everything is finalized based on laser design the most complex, and time-consumed routing is done from bond pads to connector.

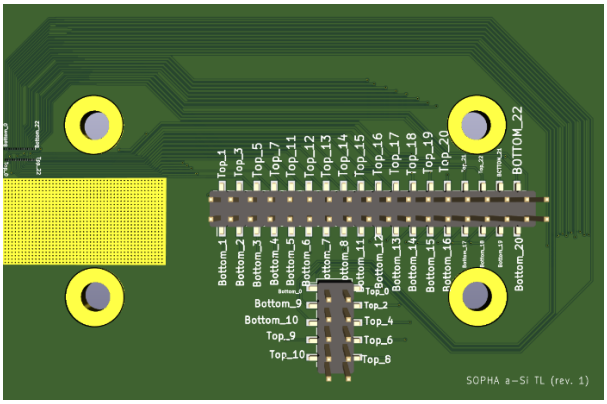

Figure 9: The 3D view of the designed PCB for aSi laser

During routing via was used between two layers of PCB to make easy routing. In the last step, the copper filling was added to the front and back layers of the PCB. The 3D image of the designed PCB for a-Si laser is shown in *Figure 9*. Similarly, the other two PCB designs were made for SiN laser and DBR bank of lasers. The in-detailed PCB designs for aSi, SiN and DBR laser are given in Appendix 1.

3.4 Functionalities of Laser Components

Before characterizing the laser, we need to understand the functionalities of each of the components used in the laser design. Using those components only we aim to get some functionalities like a large tunability, narrowest line width, high optical power, modulation, long stability of laser sources, etc. Here we will only discuss about vernier rings, Phase shifters and Sagnac loop mirrors which are the main functions of our laser design.

3.4.1 Vernier rings

To take benefit of the characteristics of silicon, tiny ring resonators have been used. An optical waveguide looped into a ring resonator which resonates when the waveguide's optical path length is an integer multiple of the wavelengths. These resonators can support several resonances, with the resonator's length determining the FSR between them. Small rings are necessary since a big FSR is preferred for many applications. [33] This calls for very narrow bend radii in the optical waveguides, which are only possible with strongly confining, highly contrasting waveguides.

A ring resonator is typically comprised of an optical waveguide which is looped and a coupling that allows access to the loop. The cavity is in resonance when the loop's waves constructively interact and accumulate a round-trip phase shift equal to an integer time 2π. With two different diameter ring resonators combine behaviour called the vernier effect. *Figure 10* shows the vernier rings effect with two rings. With coupling coefficient $\kappa = 0.3$, Both rings have their separate transmission peaks, while tuning (by heating) only one of the rings, and its spectrum shifts correspond to the other ring's spectrum. The highest optical output power is received at one of the wavelengths in both ring peaks that exactly match a single wavelength value. Which shows, this vernier ring is used as a filter.

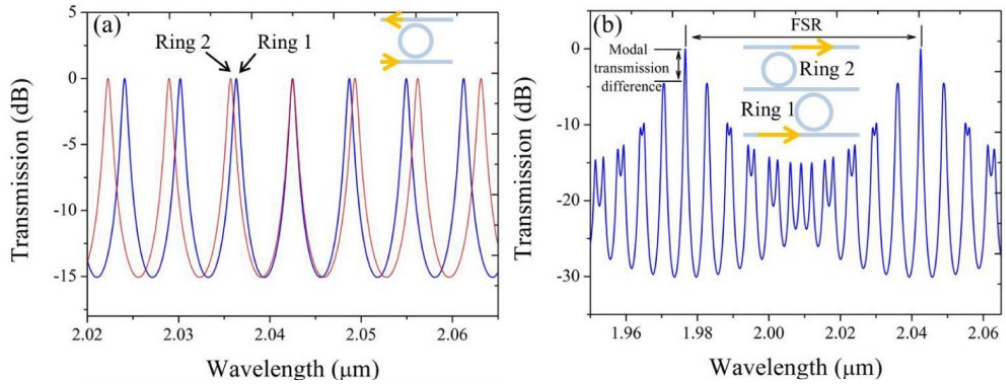

Figure 10: Vernier rings (a) Transmission spectra of two distinct micro rings with a coupling coefficient of $\kappa = 0.3$, (b) Combined transmission spectrum of two the vernier filters with FSR. [34]

The most important variable is the cross-coupling coefficient (κ), which depends on the distance between the waveguide and the ring. By simply changing κ we have different coupling powers. The large gap (distance) between the ring and the waveguide carrier gives the narrowest peak of the transmitting wavelength and vice versa. The wavelength range between two resonances or the FSR for a single ring resonator is given by the following function of wavelength:

$$\mathrm{FSR} = \frac{\lambda^2}{n_g L} \tag{2}$$

where λ represents the wavelength of light in a vacuum and L is the distance that light covers in a single round trip within the closed cavity. In this context, the group index n_g is used in the denominator referring to the group index of the waveguides, rather than the effective index n_{eff} because takes account the dispersion of waveguide. For giving example from the [34], with a κ = 0.3 and considering no waveguide loss, for the two MRRs transmission spectra with FSRs of 6 nm (for ring 1 with 31.5 μm radius) and 6.5 nm (for ring 2 of radius 29 μm) at 2.03 μm wavelength for the ring diameter of are computed and shown in *Figure 10*(a). The separate transmission peaks are somewhat moved concerning one another due to the modest differences in the FSR of the two MRRs.

Figure 10(b) displays the transmission spectra of the vernier rings obtained from multiplying the FSR amplitude of the two MRRs. The lasing wavelength of the external cavity laser is defined by the point where the transmittance is its maximum, which occurs when the resonant peaks of the individual rings align. This lasing wavelength can be adjusted by thermally shifting the position of transmission peaks. The FSR of vernier rings sets a restriction on the tuning range which is given by:

$$\Delta\lambda = \left|\frac{\mathrm{FSR}_1 * \mathrm{FSR}_2}{\mathrm{FSR}_1 - \mathrm{FSR}_2}\right| \tag{3}$$

where FSR_1 and FSR_2 represent the free spectral ranges of the two MRRs. It is possible to accomplish a greater FSR than with a single-ring resonator alone by employing two-ring resonators with differing radii. Further, we will discuss about the Thermo-optic heater widely used as a phase shifter in the laser design.

3.4.2 Phase shifters

Phase shifters (PS) are typically used to accomplish the various PIC functions. A thermo-optic phase shifter (TOPS) alters a waveguide's index (n). The PS tuning mostly relies on the thermo-optic (TO) effect. Because of the free-carrier plasma dispersion effect, electro-optic phase shifters typically offer a greater modulation bandwidth compared to TOPS. Unfortunately, free-carrier absorption causes significant insertion loss in most of these devices, The main problem is the TOPS can't be manufactured in SiN and aSi materials. Despite having a low power consumption, the phase shifter related to the opto-electro effect is difficult to manufacture. [35] Additionally, mechanical fatigue might lead to the failure of this kind of phase shifter.

The TOPS is now widely used due to its low cost, compact footprint, quick production, and simple design. The typical examples are MZI, cavity waveguide and MRR devices. One way to generate TO phase shifters is to place the heater close to the waveguide which will introduce the phase shift. Since the heater is designed to function as a resistor, adjusting its power dissipation (for example, by varying the voltage supplied to it) would alter the targeted waveguide's effective index, which will alter the optical signal's phase. Titanium nitride (TiN) metal-based substance was employed as a heater

in the design of this internal project and potential production facility at IMEC. The heater used in this project is seen in *Figure 11* shows the heater is placed to the VR and waveguide.

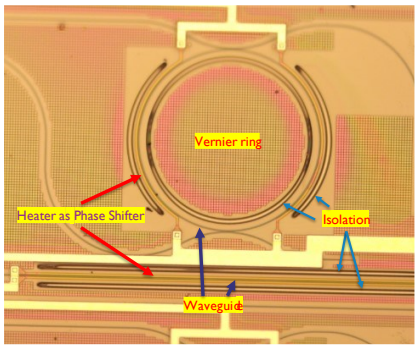

Figure 11: Thermo-optic heater as phase shifter placed at waveguide and vernier ring

In TiN-based heater devices, the necessary power to tune a complete FSR is around 20 mW, which is nearly 10 times less than in SiN-based heaters. The low-temperature sensitivity of SiN often contributes to the stability of the device. yet, TiN heater is now a solid alternative in systems that require large tunability.

3.4.3 Sagnac loop mirrors

One of the fundamental components of laser emission is an optical cavity, which lowers the mode number in the cavity and lengthens the lifetime of the photon. In general, laser cavities are made of two mirrors with different structural configurations, such as the distribution Bragg reflector (DBR), micro-ring/micro-disk, Fabry-Perot cavity by semiconductor and air index difference, and so on. Nevertheless, upon construction, practically almost all these cavities are fixed, which restricts the characteristics and application of optical lasers. [36]

Because the guided mode's evanescent tail rests on the waveguide's cladding, when light travels through a waveguide, it is not entirely contained in the waveguide core. The propagation mode of one waveguide will feel the second waveguide if they are placed near one another. As a result, the power will couple from the first waveguide to the second waveguide. For the highest coupling and maximum mode support, the field profile was separated into eigenmodes while the incident wave excites a multimode interferometer (MMI). These eigenmodes propagate at various velocities despite the absence of energy exchange, and the consequence is an interference pattern that varies throughout the length for the MMI. The MMI has the benefit of being a wideband component with excellent manufacturing tolerance. On the other hand, designing MMIs for random power split ratios is not simple, although being possible. [37] Thus, a 50/50 power splitter was used in this project's laser design, and power can be adjusted to both sides through the MMI by employing a dual-side phase shifter. *Figure 12* shows the tunable Sagnac loop mirror which has two 2x2 MMI and two-phase shifters for power splitting.

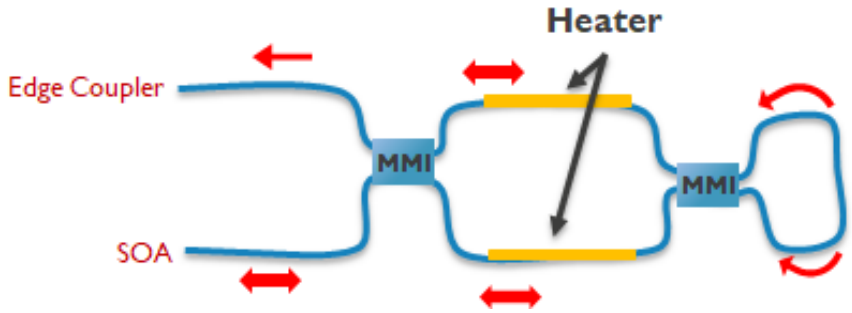

Figure 12: tunable Sagnac loop mirrors

A Sagnac interferometer is formed when a waveguide connects two ports of separate waveguides on the same side of a MMI which is shown in *Figure 12*. It represents a concept of a loop mirror with the heaters so the transmission can be tuned. A silicon substrate waveguide loop construction for adjustable reflectors coupled with an MZI. The transmissivity and reflectivity of the loop mirror may be adjusted by tuning and integrating the thermal heater with the MZI arms. Using two heaters on both arms of waveguide transmission and reflection can be controlled. Here both MMIs are considered as 3dB couplers. This means from MMI it does transmission 50-50 % power. So without heating, the mirror gives a 50-50 transmission for the same arm lengths. By heating one of the arms, the arm's length becomes longer than the other arm. So, there is a phase difference between the transmission of the light. Either we can tune one of the two heaters or simultaneously both in common and differential mode. Using these functionalities of the Sagnac loop mirror we can tune the mirror from 0% to 100%.

To get a better understanding of the Sagnac loop mirrors, with heaters in both arms, there are not many resources available on the mirror tuning based on the MMI, so we will discuss here the direction coupler-based Sagnac loop mirrors while considering the 3dB coupler. We can understand the functionality of 2x2 MMI based on the directional coupler. there is a possible four-way to operate them, In the first two ways simply tune only one arm with a heater which is shown in *Figure 13* in plots (a) and (b) where the reflectivity of the Sagnac interferometer may be adjusted from 0% to 100% in theory by adding an extra π /2 phase shift by incorporating a heater along with one arm of the MZI coupler. In Fig (e) the dotted lines in blue and yellow curves show the reflectivity behaviour of tunning arms in Fig (a) and Fig (b) respectively with different phases in radian. Fig (c) and Fig (d) show the changing of both phases together the common mode and the differential mode, respectively. Noticing that common mode phase changes have zero reflection while differential modes have several four maxima and minima in 2π radian [from fig.(e)]. While fig. (e) shows wavelength reflection in all four cases, it is worth noting that all the wavelengths are 100% reflection in differential mode and 0% reflection in common mode. And the 50-50% reflection for only one arm tunning.

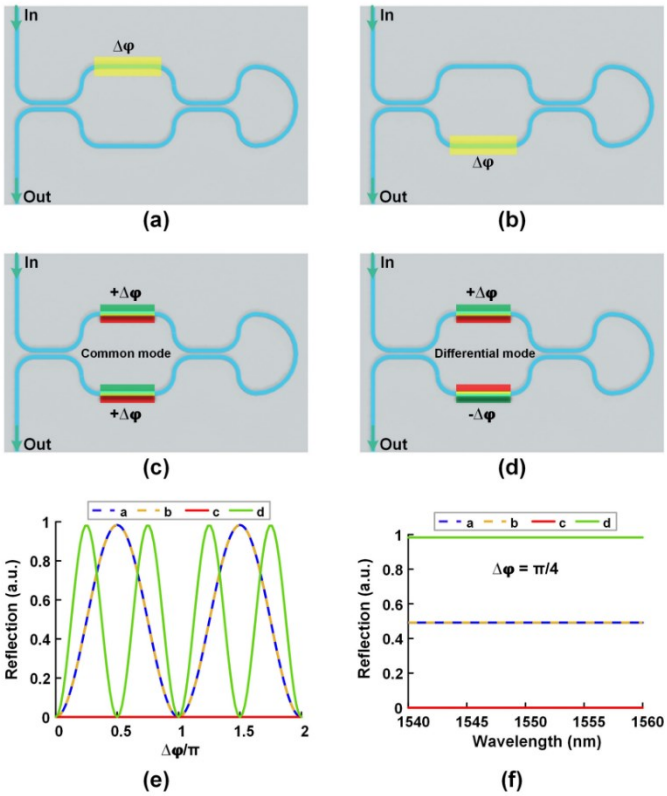

Figure 13 Tunable Sagnac interferometer with MZI coupler; (a) and (b) the tuning phase of the single arm; tuning phase of both arms in common mode (c) and differential mode (d); in (e) result of reflection vs phase and (f) results of reflection vs wavelength [38]

The phase difference Δφ between two MZI coupler arms can be adjusted externally to alter the effective coupling strength of the device. Until now we have discussed the three main tunning factors that affect the laser source. The other components like the grating coupler and Edge coupler are just for taking as light output and after fabrication no parameter can be tuned or changed, so used as passive components.

4. Characterization of III-V laser sources

In this part of the characterization of the laser we will see the cold cavity analysis, Chip cleaning and other processing, Experimental setup design and the results of the laser will be discussed.

4.1 Cold Cavity Measurements and Analysis

Initially, a passive laser cavity was fabricated on the 200mm wafer, so before the adding active laser source (SOA) into the laser die, we had a limited number of laser sources available to do µTP, so the cold cavity measurements played a critical role in the process of checking optical cavity performance after a wafer fabrication was done at IMEC's cleanroom. It is a passive cavity analysis before adding the active laser source (SOA) inside the cavity, especially the III-V-based diode source. From the cold cavity measurement, we can tell the approximate power, extinction ratio, Quality factor, Full-width half maximum (FWHM), and even tell the supported resonance modes and defects or misalignments after a fabrication that could impact the laser performance. The cavity measurement must be done for analysis of the cavity transmission without any active gain medium inside. It means determining the best cavity candidates for micro-transfer printing (µTP) to add laser sources.

The cold cavity measurement for this project is to look for waveguide characteristics of the fabricated wafer to find the narrow linewidth and high extension ratio from the different designs using cold cavity measurements. To perform the cold cavity measurement, IMEC's characterization lab has already pre-designed a system with the experimental setup. The one single laser die chip has an area of 7 mm x 2 mm in the 200mm wafer. This measurement requires several pieces of equipment and tools including a large tunable laser source (used Santac laser), an OSA, a photodetector, an optical microscope, a temperature controller (TEC), a Source Measure Unit (SMU), optical fibers for data acquisition, and three-dimensionally programmable optical wafer chuck, etc.

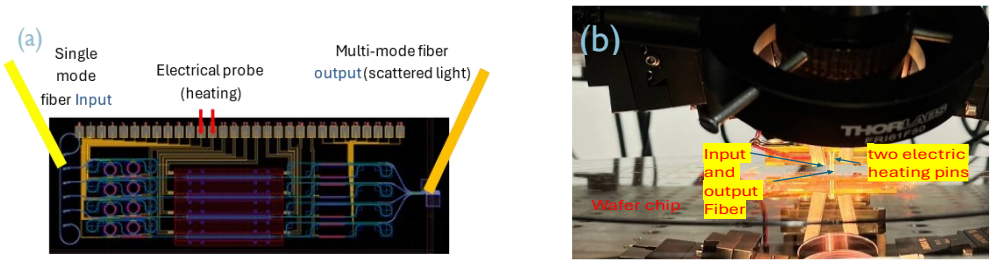

Figure 14: cold cavity measurement; (a) Schematic of cold cavity measurements of SiN laser (b) experiment setup on the lab

The wafer and optical alignment are very crucial if have to be done manually, but the optical bench and system are operated by the Python-based script program. For the cavity analysis, the long wavelength spectrum of the continuous laser was injected using single-mode fiber through the grating coupler and the output scattered light was taken with multimode fiber at the edge coupling side. During this transmission process, only one of the vernier rings was tuned using the heater. The schematic for the measurement shown in *Figure 14*(a) and *Figure 14* (b) shows the experimental zoom image of the two heater pins for tuning and two optical fibers for input and output.

During the analysis, all the lasers designed for this project were analyzed. The vernier tuning with the heater was necessary for this analysis and since the pitch size was fixed so electrical probe pins have limitations for checking all the cavities due to practical pin distance issues for only aSi laser. So, for these lasers, the entire wafer was heated which resulted in both rings being tuned. The experimental setup and the components used for a cold cavity measurement are shown in *Figure 15*.

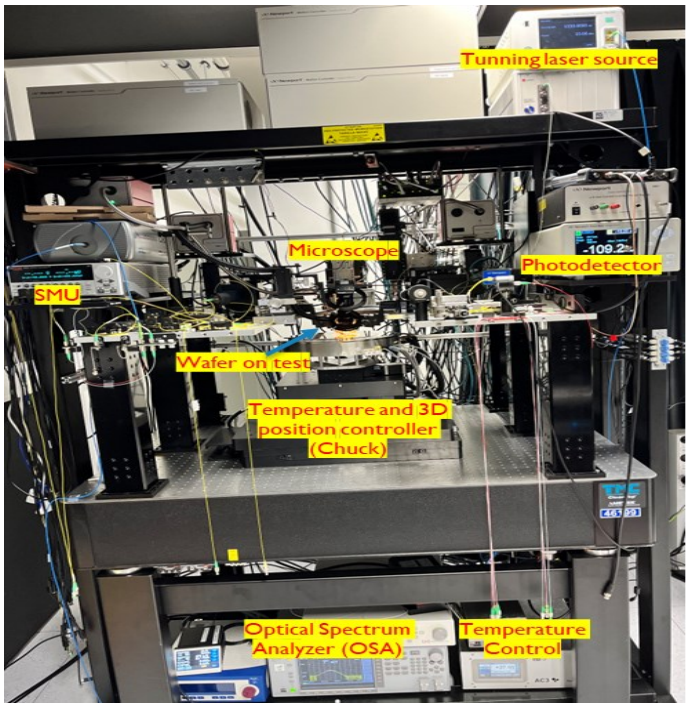

Figure 15 Cold Cavity Measurement setup used in the laboratory

The electric probe is used to inject current from bond pads and heat to one of the vernier rings to tune its output. The peak of the ring gets shifted to wavelength peaks via heating (shown in the vernier ring *Figure 10*). The heating simply changes the material's refractive index and its length, so the ring resonator output has also shifted. When both rings individual peaks perfectly match where output is in the lasing medium, and light propagates through the cavity to the EC output. The result of the cold cavity measurement for the aSi and SiN laser is discussed following:

As from the *Figure 16* (a) shows the combined spectrum of all four tunable SiN lasers. Based on the all laser-designed output is from the edge coupling side so there is only one way to detect scattered light from the designed trench. For SiN measurement, we observed scatter light, so the detected power is quite low as can be seen from the spectrum. But the most important thing we want to see from the spectrum is the extension ratio of the transmission output and the approximate linewidth of the laser output. The FSR of the SiN lasers is 2nm but from the full spectrum did not get information about how broadening of the single wavelength (which means the width of the peak wavelength). The SiN-1 laser can have the highest power and SiN-4 can have the lowest power with many modes of SiN-1.

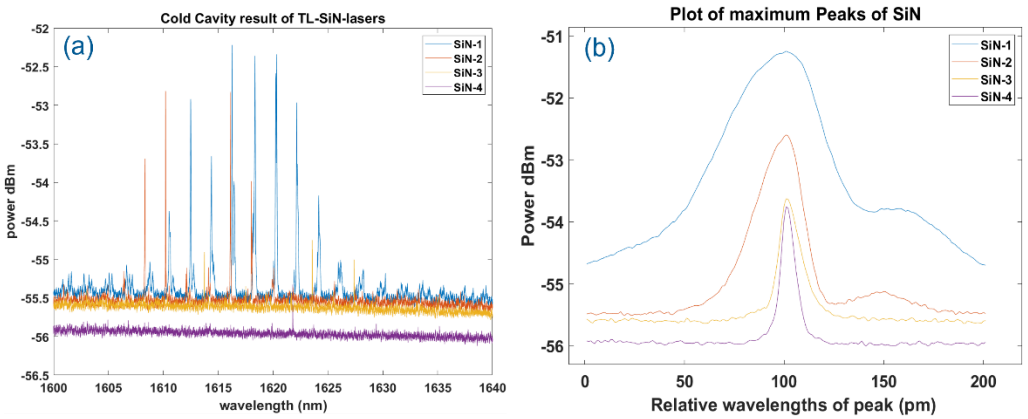

Figure 16 (a)Cold cavity measurement result of tunable SiN laser, (b) maximum Peak wavelength plotted of all lasers at point 100.

To get information for the width from the spectrum, additional data analysis was needed. *Figure 16*(b) shows the filtered plot around the peak wavelengths. For all four spectra, taken the maximum peak value and placed at point number 100 and then both side additional 100 points were plotted which means a total of 200 wavelength points are plotted on the x-axis. The chosen 200 points are only purpose to cover of the full wave of the peaks to compare with other laser peaks for all four SiN lasers. From the result, we can see that the SiN-3 and SiN-4 lasers have the narrowest linewidth of the peak, and these two lasers were used for the micro-transfer printing method to print SOA for making lasers.

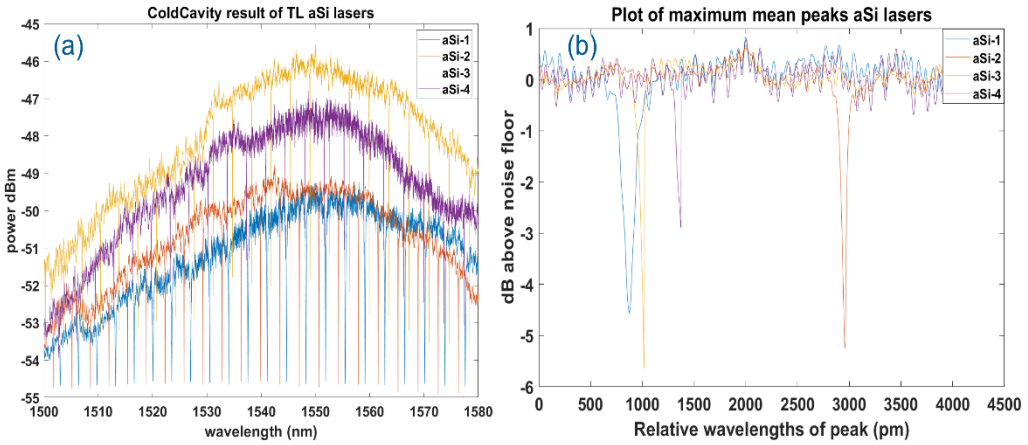

Figure 17: (a) Cold cavity measurement result of tunable aSi laser, (b) The mean plot of maximum peak wavelengths plotted of all lasers above the noise floor

For the aSi laser, the cold cavity results are shown in *Figure 17*(a) from the plot we can tell the peaks are inverted than the SiN laser output power and that can be explained by the light transportation opposite than SiN laser. The FSR of the aSi laser is 3.5 nm which can be verified from the peaks. When it matches the lasing condition there that wavelength is filtered out and that can be seen in *Figure 17*(a), Here we also look for the linewidth and the extinction ratio of the lasers.

For getting information about the line width of the peak wavelength again the same technique was used to plot only a few data points near the peak. But here due to high

noise in all peaks data, to overcome the noise the mean is applied and made the same reference line. *Figure 17* (b) shows the mean power values in dB versus the number of wavelength points used to cover all the peak values. From the plot, I can tell that aSi-2 and aSi-3 lasers have the highest extinction ratio and the narrowest line width of the laser peak.

Based on this cold cavity measurement, concluded that from the four SiN lasers, The SiN-3 and SiN-4 lasers have the narrowest peaks from the plot. While for the aSi laser, aSi-2 and aSi-3 lasers are good in terms of extinction ratio and narrow linewidth. Further based on these data the micro-transfer printing was done with the collaboration of Ghent University and the chip was received after the SOA was printed on the lasers. Now further we will see the brief process of chip cleaning, dicing, microscopic analysis, and packaging of lasers.

4.2 Chip Dicing, Cleaning, Testing and Packaging

After the Micro-transfer printing process, the piece of the die was received in batches. As for the first batch, it has limited printed laser sources for analysis to check if every process goes well and the laser is working. During the µTP process together with SOA printing, the gold (Au) metallization was also done. The bond pads and other wire connections are fabricated with Aluminum (Al) at IMEC during wafer fabrication. The first die sample is shown in *Figure 18*, because many samples look the same so unique identification is necessary, so to identify each other separately the alphabetic name was given for convenience. The first die has two copies of it, called samples S3 and sample S4. The first two samples S1 and S2 were damaged. The red squares and alphabetic names show the location of the SOA printed. The yellow line shows the dicing request to finely cut those lasers separately for further processes.

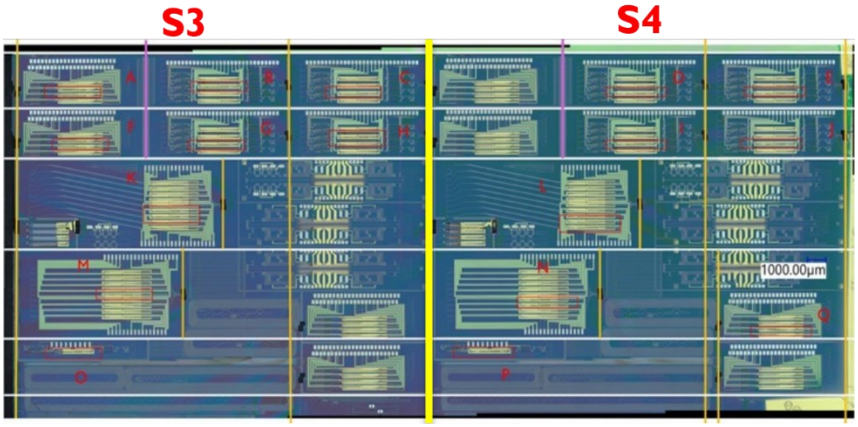

Figure 18: 1st batch die of samples S3 and S4 with named (red) and diced (yellow)

Before sending to dicing of this die the commercial Ix845g positive photoresistor was added on top to make devices safe during the dicing. After dicing the wafer die, the individual laser chips were kept safely in the jelly-like box where they were fixed, the box provided safety and ease of transportation. *Figure 19*(a) shows the two laser devices A and F placed in the box. The immediate step after the diced chips is to remove the photoresistors from the top surface which were added before the dicing process. To remove the photoresistor following standard chemical cleaning process was used for the laser chips. The individual laser diced chips were baked for 2 hours at 80°C in the Technistrip Micro D2 chemical which is commonly used for removing photo resistors.

The process follows bake in Isopropyl Alcohol (IPA) for another 20 minutes at 50°C. Further steps were rinsed multiple times in the three solutions starting with Acetone, deionized water (DIW) followed by IPA. *Figure 18*(b) shows the baking of four different chips and names used on paper for references to identify each device. After the cleaning, further microscopic analysis was needed. it is important to check for lasers after the cleaning step, sometimes if there is an extra layer or piece left it is needed for another cleaning batch. For the microscopic analysis, both horizontal and vertical sides were checked, the vertical side has edge coupling and laser light will come from the edge. some photos were also captured as a reference for later comparison if something got damaged. *Figure 18*(c) shows the vertical microscopic analysis.

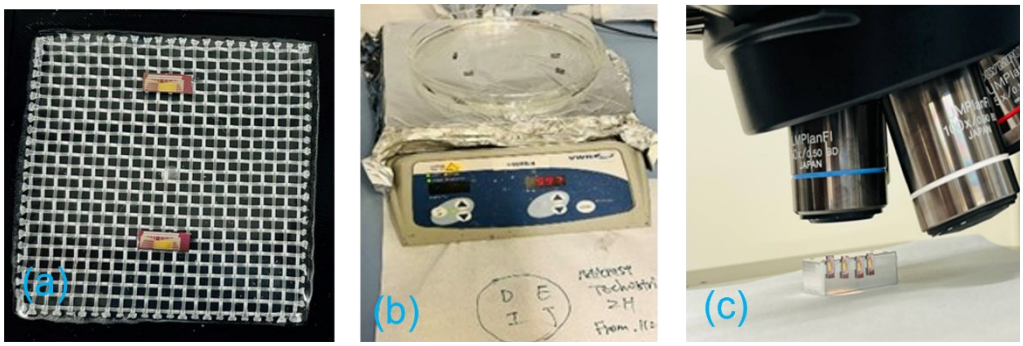

Figure 19: (a) Diced chip in the package box, (b) Cleaning photoresistor from the chip, (c) vertical chip observation under the microscope

Further electrical characterizations of the laser chip are necessary, probe station setup of IMEC's B lab has been used. The electrical connection and SOA diode response play a significant role in the behaviour of lasers. The chip was placed on the vacuum chuck and a tiny electric needle was used to probe the respective bond pads. These probes are connected with SMUs to inject and measure the voltage and current values from the bond pads. The vertical microscope is used to observe the device during pin probing. It plays a vital role in making good connections between the needle and the bond pad. *Figure 20*(a) shows the measurement of the chip, and several needle probes connected to the bond pads and the top screen shows the microscopic image of the chip and pins connected by a needle which appears as a black shadow.

From the analysis result, it shows most of the components are well-connected but for some, the laser's SOA is not connected to the bond pads which means there is a connection issue between SOA and bond pad wire. From this analogy, It is concluded that the device that is working on pads and showing high SOA resistance on bond pads due to two different metal joint contact. *Figure 20*(b) shows the behaviour of SOA on the bond pads versus measured direct on-SOA gold metallization. Here two devices E and J are shown which measured and compared I-V characteristics from Pads and direct from the SOA. Comparing the current value of device E on SOA (red) vs on Pads (magenta) at 1.5 volts. If comparing the same measurement of device J on SOA (blue) and on Pads (green) at 1.5 volts. It concluded that through the bond pads resistance was highly increased to more than a double.

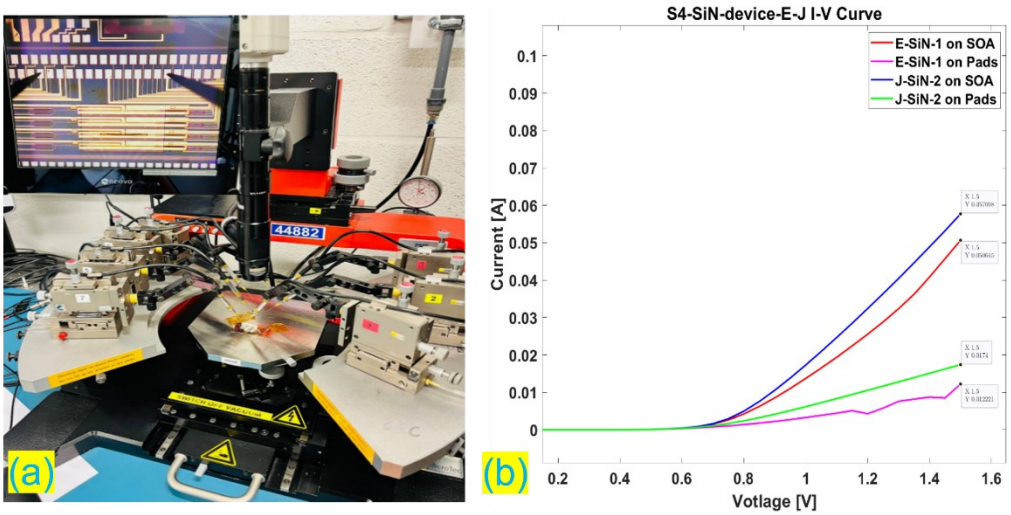

Figure 20 (a) Electrical characterization on the probe station, (b) comparison of current for Laser E and J on Pads vs on SOA

It was noticed that there is a large resistance present between SOA and bond pads and that is due to the two metal Au and Al connection joints. The comparison of the degradation of the current while measuring from bond pads and SOA suggests making an additional bridge between SOA and bond pads, it was tried with metal connections and silver paste to electrical connect, but it did not work out due to the very small size of metal wire and small SOA metallization width. In the laser packaging step next, the wire bonding process is followed. The wire bonding on the designed PCB was done by the IMEC wire bonding experts team. For SiN laser glob top is also applied to get protection from unwanted wired damages. For the aSi due to the long wire length, we avoided the glob top.

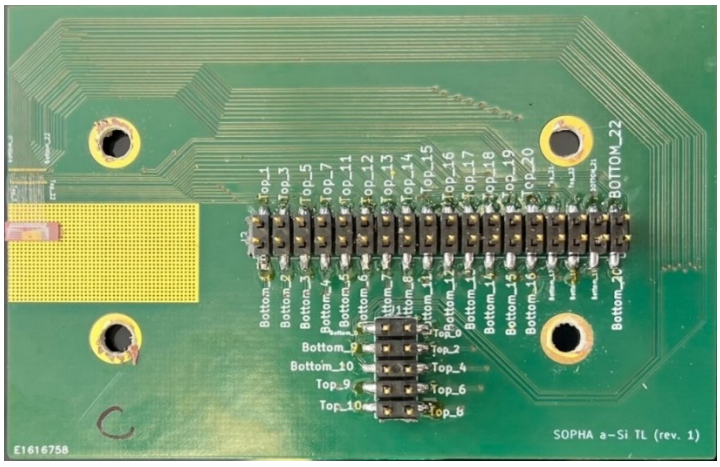

Figure 21: A wire-bonded and soldered connector for aSi on the PCB

The laser chip was placed on the heatsink during the wire bonding. After the wire bonding the SMD connector soldering was done to connect those PCB pins from where external electronics circuitry will be operated. *Figure 21* shows the final image of the aSi laser on PCB after wire bonding and soldering which was used for the characterization of the setup. Similar steps were followed for SiN lasers as well.

4.3 Experimental setup design for laser characterization

For integrated chip characterization, it always has a special setup required based on their design. The lasers used for this project are edge coupling types and this was the first time designed and tested at IMEC. To work with each of the functionalities of the single laser, there are some basic component requirements from the laser design, each laser has two heaters for tuning rings, two heaters at the sagnac loop mirror, one phase shifter, and one SOA, so in total six Source Measurement Unit (SMU) are required to inject and simultaneously measure the voltage or current. Three Keithley's 3rd generation two-channel 2600B series SMUs have been used for this project. To measure the output light, from the edge side multimode fiber was used to get maximum coupling, while from the GC side, it is designed to use a single-mode fiber. The electrical connection from SMUs to chips and the BNC connector rack has been made and labelled with respective devices. Figure *22* shows the schematic of the measurement of laser testing, orange squares show the electrical pins connection to the laser. The setup is temperature-controlled to 15°C. The edge coupling laser output is separated into two parts 90% of the power goes to the OSA for spectrum analysis while 10% of the power goes to the electrical spectrum analyzer for noise calculation.

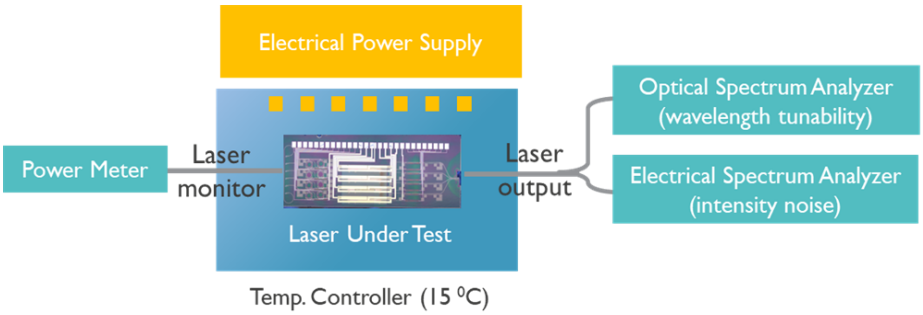

Figure *22:* Schematic of the laser under test with temperature controller (TEC)

The motorized controller based on two XYZ translation stages on the optical bench was used to get full functionality for two fibers. These rotating stages were very useful during approaching both couplings on the setup. The goniometer in the translation stage is also useful for changing the fiber angles. Between the two translation stages, the temperature controller was attached to the Z-translation stage, for moving vertically. The optical microscope with a light source was also fixed vertically with XYZ translation to focus on the lasers and fibers during coupling. The photodetector (PD) was used for optical power measurement, it is connected to the digital power meter.

The temperature on the bench was set to stay 15°C with TEC and the on-chip laser PCB was placed and screwed on the chuck, the back side of the PCB is a copper plate that is connected to the temperature controller chuck. A careful connection was made between the respective pins of SMUs to the laser because SOA is very sensitive to the current and mistakenly high power easily burned the SOA. So before turning ON devices first, limit the supplying current and power by all the SMUs so it does not reach by mistake higher power and prevent the device from being damaged.

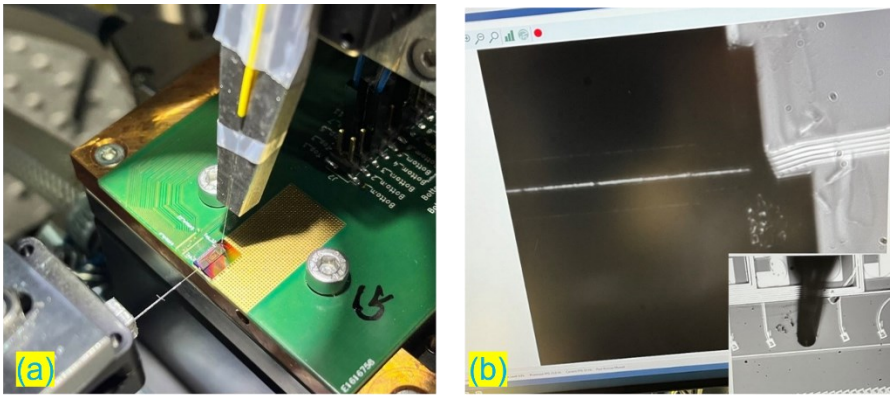

Figure 23: EC and GC coupling; (a) shows the EC and GC on the Chip used in the lab, (b) Microscopic image of the EC and grating coupling (bottom right image)

In laser characterization, the critical part is to do grating and edge coupling with the fibers. The alignment of the fiber was crucial and essential. *Figure 23*(a) shows the edge coupling and vertical coupling for the aSi laser-G and *Figure 23*(b) shows the microscopic image in the desktop after the maximum power coupled for the laser.

Figure 24: The Experimental setup used for the characterization of lasers

For the characterization of lasers, it is more convenient, fast and efficient to operate SMUs and OSA by Python-based script. With the help of my co-supervisor Liwang, the

very crucial code was developed and devices were operated remotely using the code. The lab experimental setup used for the characterization of both aSi and SiN laser sources is shown in *Figure 24* and the bottom right picture shows the magnified image of the laser test on the Chuck. Now further we will discuss the results of the devices that were tested.

4.4 Test results of the SiN lasers

As for the design, there were four SiN lasers in a single chip and from the first batch S3 and S4 samples contained a total of 8 SiN chips. However, each chip has only one SOA-based laser source available for testing and after the electrical characterization tested on the probe station, the 4 devices in S3 die B, C, G, and H the SOA were not working from pads due to electrical contact issue between two metals. (which means can only work from the SOA). On the left four devices in sample S4 were electronically working (especially SOA) from the bond pads, so wire bonded them and tested them on the optical characterization setup. If all the processes until now were good, then we should have the working lasers. But unfortunately, all four SiN lasers did not give the laser wavelength although it is giving optical power but no lasing. By tuning the laser functionalities (including phase shifter, vernier rings, and loop mirrors) we might reach to lasing condition but after tuning all the functionalities we don't able to see the lasing output.

The light source SOA behaviour is the most important for the laser, so the measurement was to look at the SOA performance with sweeping current till the 200 mA and compliance voltage limit was set to 3 V. So, the maximum electrical power SOA will not reach beyond 600 mW because higher electrical power simply burned the SOA device and after that, our device has no use. The characterization was done for 4 SiN laser devices named D, E, I, and J. All these lasers show almost similar behaviour.

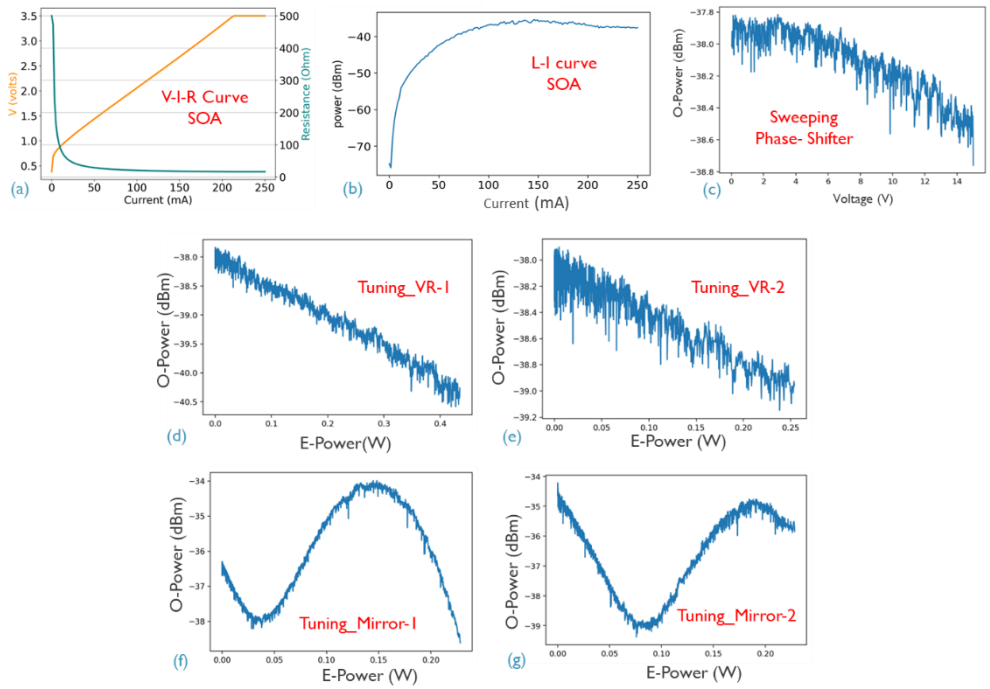

Figure 25: Tested results of laser device-D; (a) VIR curve of SOA, (b) O-power vs current (mA) of SOA, (c) O-power vs voltage of phase shifter, (d) O-power vs E-power of tuning VR-1, (e) tuning VR-2, (f) O-power vs E-power of tuning mirror-1, (g) tuning mirror-2.

Figure 25 shows the sweeping measurement of laser D. where *Figure 25* (a) shows the measured voltage-current-resistance (VIR) curve of the SOA, and the yellow line shows the behaviour of voltage with the current. it simply shows the voltage linearly increasing with the increasing current. The curve reaches saturation when voltage reaches 3.5 V which is the safety voltage for the device. Blue lines show the I-R curve and exponentially decrease the resistance by increasing the current and reaching a saturation resistance of around 20 Ω.

Fig-25(b) shows the response of optical power (O-power) vs supply current to the SOA, the optical power increases with increasing current till 100 mA and after power reaches the saturation further increase might decrease the output optical power. (c) shows the optical power (in dBm) vs voltage sweep (0-15V) of the phase shifter (PS), By tuning the PS ideally, we should see the tuning of different modes of lasers but unfortunately, I didn't see any major changes in optical power with phase shifter tuning. The phase shifter is mainly used for fine-tuning of the wavelength. (d) shows the response of O-power vs electric power (E-power) of tuning vernier ring (VR)-1, and (e) shows the O-power vs E-power of tuning of VR-2, Ideally by tunning any one of the rings it should give lasing with respective wavelength spectrum of the other ring but tuning both of the rings doesn't give laser and just O-power drops with increasing E-power. (f) shows the O-power vs E-power of tuning mirror-1, and (g) shows the O-power vs E-power of mirror-2. Similarly, by tunning one of the mirrors it might match the lasing condition inside the cavity, and ideally, we should see several modes in the output optical power but here we simply see the one large mode that does not give any lasing. Further, we will see some possible reasons for not giving the lasing. Next, we see the characterization of aSi laser.

4.5 Test results of the aSi lasers

The aSi laser design had even fewer devices to test than the SiN lasers from the first batch. Out of five devices, two devices had electrical connection issues from the bond pads like in SiN lasers and one device did not give any optical output still after the extra cleaning.

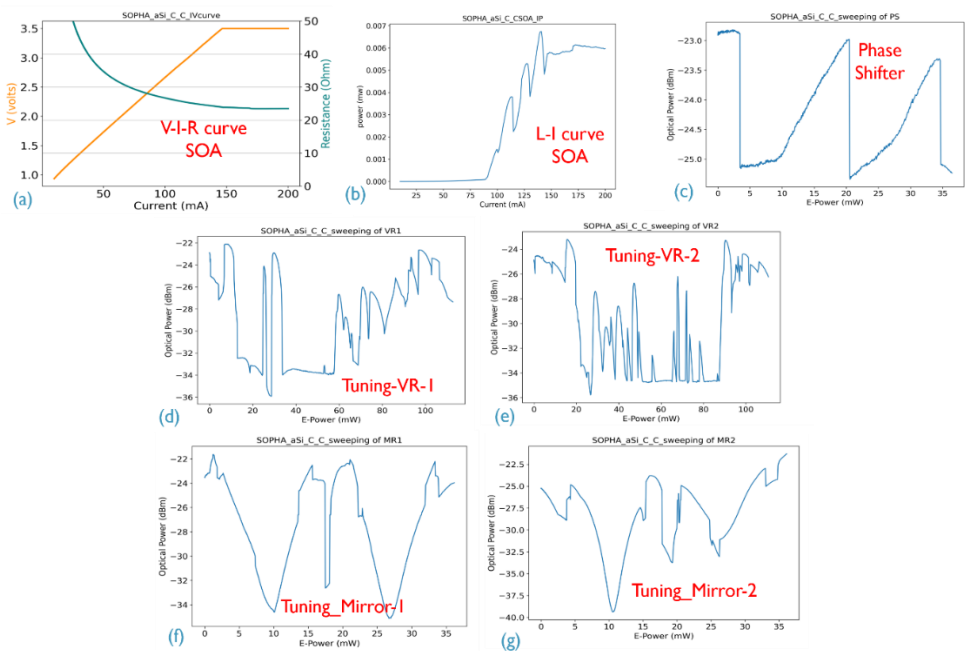

Figure 26: Tested results of aSi laser device-C; (a) VIR curve of SOA, (b) L-I curve of SOA, (c) sweeping voltage of phase shifter, (d) tuning VR-1, (e) tuning VR-2, (f) tuning mirror-1, (g) tuning mirror-2.

From the rest of the two, only one device was working which means it matched the lasing condition and gave a laser. it had a peak wavelength of around 1580 nm. For this working laser, *Figure 26* shows the behaviour of SOA, tuning Phase shifter, both vernier rings tuning and two mirror tuning. By comparing both *Figure 25* and *Figure 26* we see the difference between the working and not working device behaviour. Noticing *Figure 26*(b) the L-I curve of SOA has multiple modes although the output power is not very high. One way of approximate guessing to check if the laser will give a lasing spectrum is by seeing from its L-I curve. So, this is a valid way to see the optical power output while sweeping the current of SOA. The (c) shows the plot of O-power vs E-power while voltage sweeping of the phase shifter, from the curve sees periodic mode changing. While tuning both vernier rings results are shown in (d) and (e) with O-power vs E-power. By tuning vernier rings we expect to see the clear periodic wavelength modes and FSR of the rings but here the rings' behaviour was not isolated from other components so there is an influence of mirrors, phase shifter, and the thermal effects can cause this fluctuation and not giving the periodic behavior but important to notice that we can tell from O-power changes there are many wavelengths are changing during tuning rings. While (f) and (g) show the result of O-Power vs E-Power while tunning both mirrors. For the mirror, it also does not have any periodic mode-shifting behavior, but based on O-power fluctuation there are some lasing peaks present. *Figure 27* shows the optical spectrum of the aSi laser output of device-G of 1582 nm peak wavelength. For this laser, it is quite distinct the peak wavelength above the noise floor and we can see the side mode suppression ratio which is nearly 40 dB. Also, the linewidth of the laser is quite narrow. This peak has a linewidth of approximately 0.3nm.

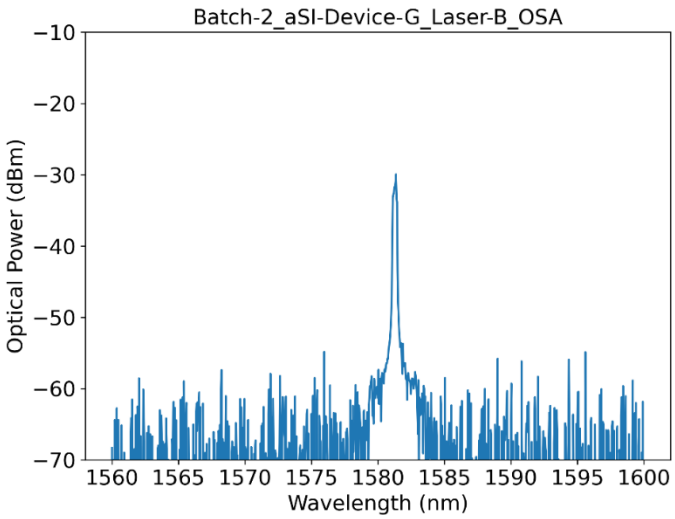

Figure 27: The optical spectrum of the Laser output of aSi Device-G Laser-B

For this working laser further, we will see the tunability of the laser by tuning different components of the device and also the supported modulation of the laser.

4.6 Wavelength Tunability of Lasers

For the wavelength tuning, we have vernier rings, mirrors, and phase shifter components to play with and see the tuning ranges supported by the laser.

Unfortunately, this device was burned while tuning the mirror-1 so I have no result of fine-tuning of the phase shifter. So, I will only discuss vernier ring tuning and mirror tuning.

4.6.1 Vernier rings tuning

To tune the wavelength the most effective way is to tune the vernier ring with electrical power sweeping. By tuning a single ring, we can also get the large wavelength tunability. *Figure 28* shows the individual tuning graph of vernier rings. For the aSi laser B, the peak wavelength starts to tune from the central wavelength of 1580 nm. In *Figure 28*(a) and (c) show the full tuning wavelength range while tuning only one ring to another. It tells that both plots show the laser wavelength can tune from 1555nm to 1625nm. But to get the information about how wavelength is sweeping with the tuning voltage is shown in (b) and (d). From the heat map, I can tell that both rings have opposite behavior and VR-1 initially starts to decrease its wavelength till 1555nm at 5 volts and then makes a sudden jump in wavelength to 1625nm, and from there, it starts to again decrease with further increase of voltage more than 5V.

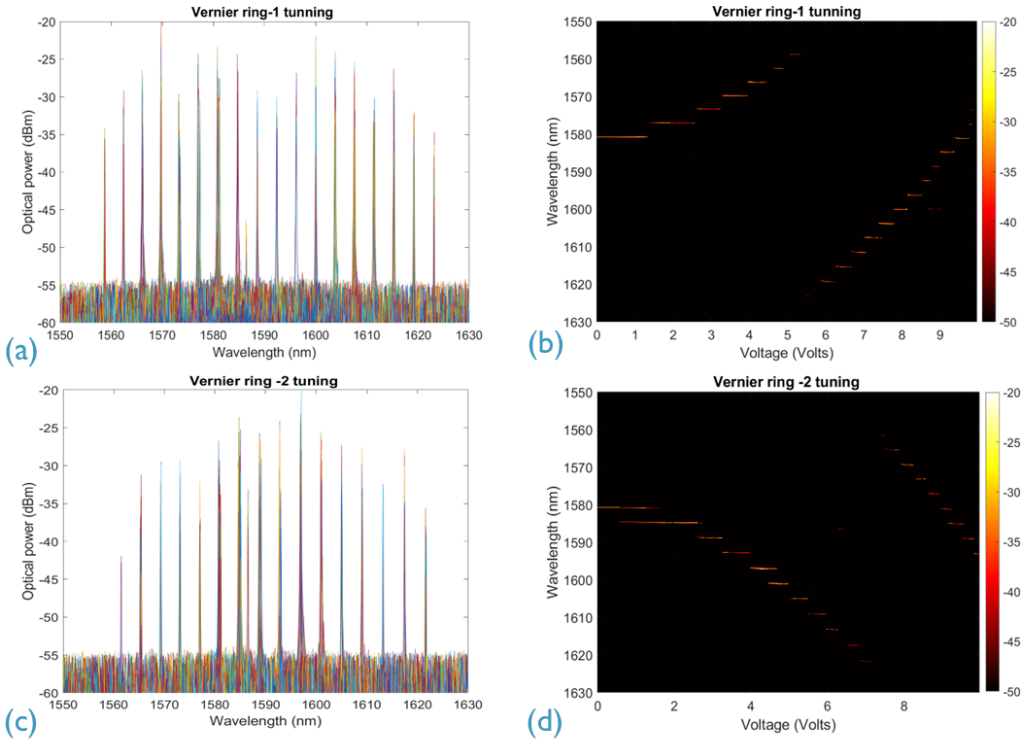

Figure 28: aSi laser-B tuning vernier rings; (a) wavelength tuning of VR-1, (b) heat map of tuning VR-1 with voltage sweeping, (c) wavelength tuning of VR-2, (d) heat map of tuning VR-2 with voltage sweeping.

Regarding VR-2, it behaves exactly opposite to VR-1 and the peak wavelength starts to shift to the higher wavelength until around 1625 nm till the 7.8 volts, then makes the sudden jump in wavelength to 1555nm and increases in wavelengths with further voltage increasing. The discrete spots appearing in the heatmap show the wavelength jump while both rings' peak wavelengths are matched. This behaviour perfectly matches the vernier ring behaviour discussed in the laser functionality part.

4.6.2 Tuning of Mirrors

As discussed earlier, another way to see the tunability of the laser device is to tune the Sagnac loop mirror used in the laser. The main purpose of the loop mirror is to set the reflectivity between the cavity and edge output. But here tried to tune both mirrors individually to see the effect on wavelengths. *Figure 29* shows the result plots of tunning mirrors. Which (a) shows the voltage sweeping on mirror 2, which shows the wavelength shift is not quite separated around the 1585nm so many wavelength peaks overlap in very few nanometers. Only one wavelength was shifted to 1580nm at 3 volts shown in the heatmap.

As for sweeping mirror-1, while running this experiment maybe I made some mistakes in lowering the voltage of mirror-2. So, during running this measurement our laser SOA was burned. The possible thought of giving both mirrors at high voltage makes high reflection in the cavity and optical power is building up inside the cavity. The plot (b) is also similar to the mirror-2 result but here so many green lines are simply considered as noise and the heatmap also sees the continuous wavelength peak at 1585nm while sweeping the voltage. The optical output power also starts to decrease with MR-1 tunning. The optical vs electronic power response of the mirror tuning is shown in *Figure 26*(e) and *Figure 26*(f). By tunning these mirrors we didn't get much wavelength shifts.

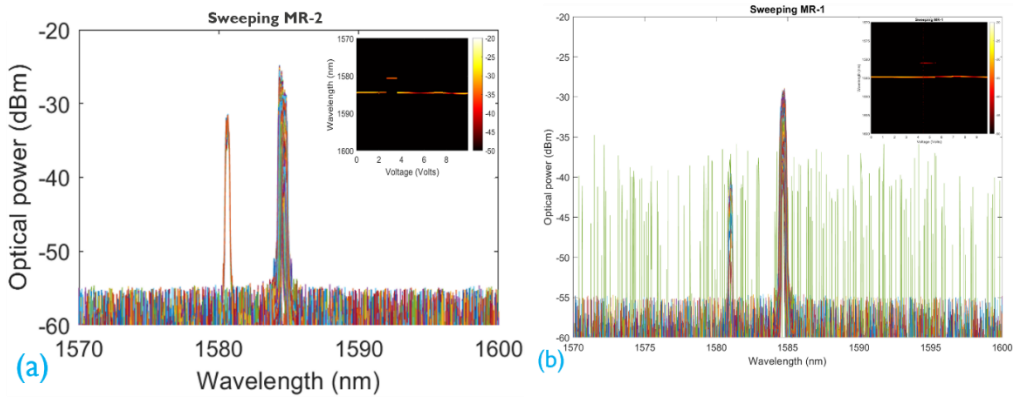

Figure 29: Tuning of mirrors; (a) tuning mirror-2 with heatmap, (b) tuning mirror-1 with heatmap

As this device's SOA was burned during mirror-1 sweeping, I wasn't able to perform the sweeping of the phase shifter for fine-tuning the wavelength. So for the modulation of the lasers experiments, I have used a second batch of lasers. For the second batch of lasers again repeated the same process which followed for the first batch of lasers. After finishing every process again this second batch has a two aSi laser working. So further modulation analysis was done with those lasers.

4.7 Modulation of the Lasers

As we know modulation plays a crucial role in the PAS experiment and for PAS, we need low frequencies in a few KHz due to the sample relaxation time being a few milliseconds for the PA signal. So, we have seen the modulation behaviour of these lasers. For the laser modulation experiment, the function generator is used as the power supply for SOA, and the edge laser output was recorded on a photodiode which converts optical power into an electrical signal and this electrical signal is analyzed in the oscilloscope. The DBR laser has been used for this modulation experiment. There few ways of

modulation that can be done the power ON/OFF modulation, the gain modulation tune between the lower laser threshold to the maximum saturation power, and the small signal behaviour of this laser. Also, the output power response during frequency modulation is quite important to look at for these lasers. After this analysis, we can be able to tell if this laser can be used for PAS measurement or not. Here we will only see the power ON/OFF modulation and small signal sine wave modulation.

For ON/OFF modulation we can use sine wave and square wave. *Figure 30* shows the sine wave laser modulation, where (a) shows the oscilloscope image at three different frequencies of 10KHz, 100KHz, and 500KHz. The laser output is shown in a dark blue color and the reference voltage signal is shown in a light blue color. At lower frequencies laser output stayed high and constant and it started to decrease after reaching several KHz frequencies. while (b) shows the plot of sine wave modulation as power vs frequency response. From the frequency response, we can see that after 10KHz, the laser power starts to decrease further to higher frequencies. The laser output is very negligible from 500KHz, the modulation limit for power is defined at 3dB point for this device it is nearly 100KHz. It is also noticed that our reference signal power starts to increase after 100KHz and that we see the nonlinearity behaviour of the laser. In conclusion, sine wave modulation behaviour is stable and higher for the lower frequencies which is needed for the PAS experiments.

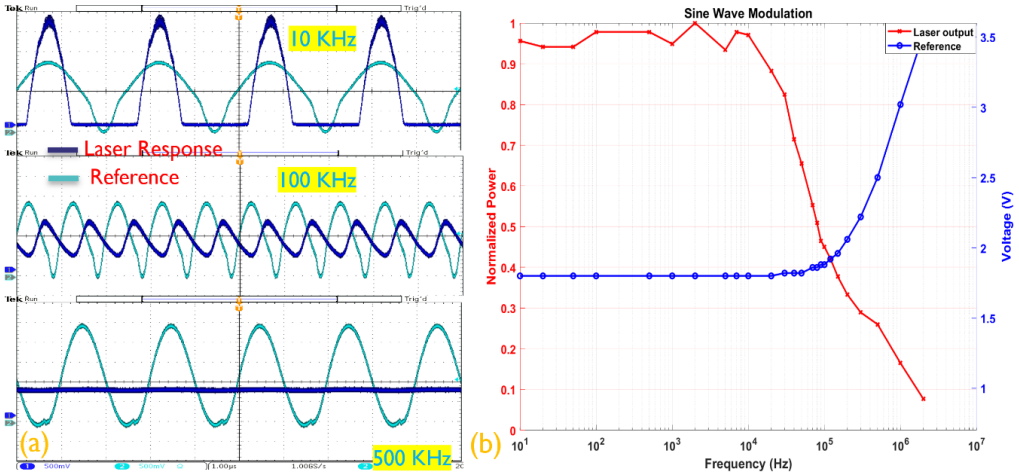

Figure 30: Sine wave modulation; (a) oscilloscope image of frequencies 10KHz, 100KHz, and 500KHz, (b) Sine wave frequency modulation response of laser and reference voltage

Further, we can see the square wave ON/OFF modulation response. *Figure 31* shows the square wave modulation response of the laser. (a) shows the oscilloscope images at frequencies 10KHz, 100KHz and 500 KHz. While (b) shows the square wave frequency modulation response. The red line and left Y-axis show the laser behaviour with frequency while the right Y-axis shows the Reference voltage behaviour with frequency.

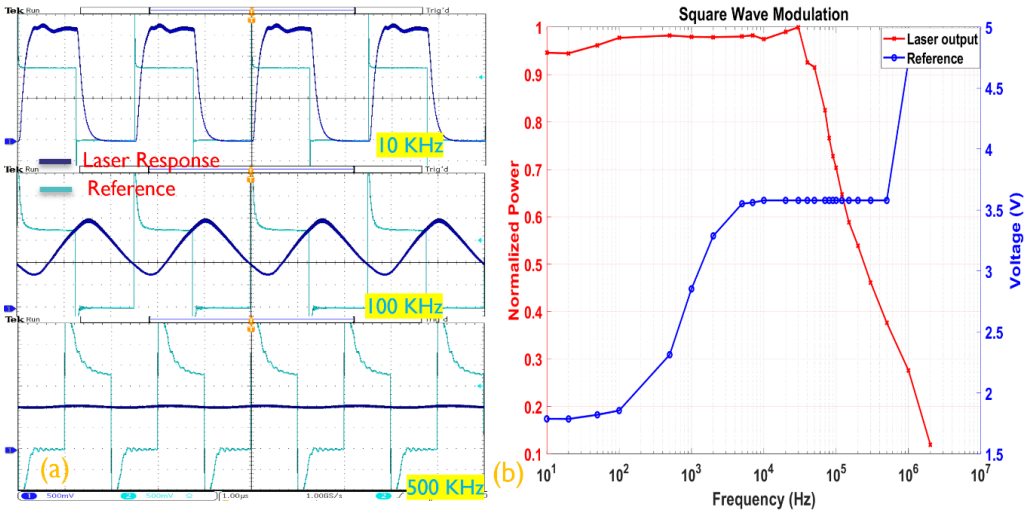

Figure 31: Square wave modulation; (a) oscilloscope image of frequencies 10KHz, 100KHz, and 500KHz, (b) Square wave frequency modulation response of laser and reference voltage

The square wave modulation response also starts to decrease after 100KHz frequency. The reference signal continues to increase with higher frequencies which is As in *Figure 30* and *Figure 31*, both sine and square wave frequency behaviour look similar for the frequencies of 10KHz, 100KHz, and 500KHz with a maximum modulation limit is 3dB from the peak which is here 200 KHZ. Based on both modulation responses, I can conclude that this laser is compatible with both sine and square waves with a frequency limit of 100KHz. For the square wave, we have higher shape distortion than the sine wave single.

It is very important to analyze the small signal modulation behaviour of these lasers. *Figure 32* shows the small signal sine wave analysis of the DBR laser. From the plots, I can say that normalized power is not much affected by increasing frequency. Which is the opposite behaviour from the ON/OFF modulation seen above.

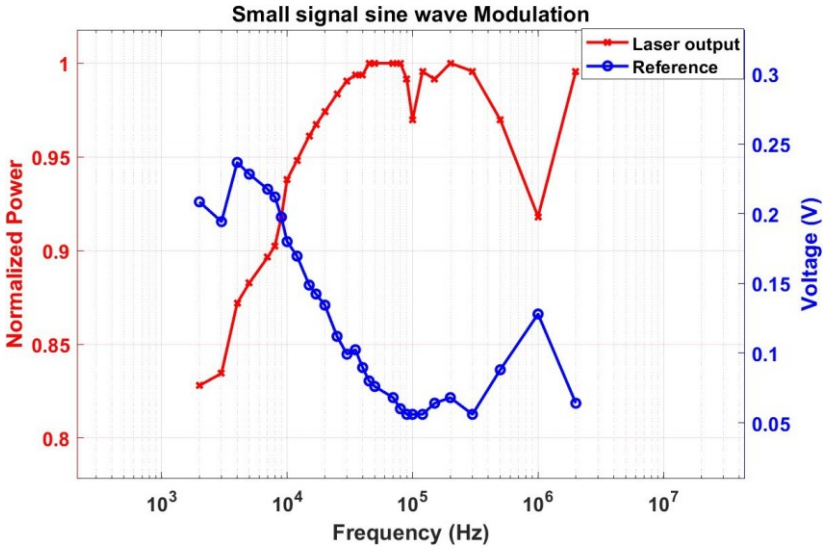

Figure 32: Result of small signal sine wave modulation response of laser and reference voltage

After the laser reaches high optical power (saturation) the 200mV peak-to-peak reference voltage was applied as a small signal. The behaviour with the frequency normalized power behaviour can be seen from the left y-axis and reference voltage in the right y-axis. This result has a bit of fluctuation due to temperature and other component effects in the laser. Due to the function generator limit, I can't go beyond the 20 MHz but ideally, the small signal behaviour has a maximum cut-off frequency in several (> 25 MHz) MHz. That is explained by the nonlinearity of the lasers. So in conclusion using ON/OFF modulation (with a large signal) has laser bandwidth in the KHz range while small signal modulation has a very large bandwidth in several MHz.

4.8 Possible reasons for the laser devices not working

The reason behind some tunable aSi and SiN lasers not working is extremely hard to conclude and at the same time also extremely difficult to find the single or multiple reasons why it is not working. Due to time constraints, I could not proceed with further analysis to find the reasons for these not working devices. But there few things that might be possible reasons for these not working devices:

Micro-transfer printing technique: This technique could be the first and main reason for the not working devices. Because this technique is still in the R&D phase and from last few years imec has started this technique for printing this kind of SOA to chip for lasers. This technique is mainly used here for LED array sources and these III-V coupons are manually placed, so mostly the issue can arise from the light coupling between III-V material to aSi material. The slight mismatch between two tapers for SiN laser (the first taper between III-V to aSi and the second between aSi and SiN waveguide) can drastically affect the lasing performance. So, by improving this technique, we might have many working devices and use this method for injecting III-V material into Si wafers.

The SOA light source: The SOA-based coupon-making process is quite complex and uncertain with managing the concentration of III-V materials with a few nanometers of quantum wells. Although the coupons for 1525nm, 1550nm, and 1575nm are widely used and successful, there is still an issue for some of the sources. Even during this project's laser testing, the SOA-based laser sources for 1675nm wavelength were not working.

Based on Laser Design: As this laser design was the first time used and explored at imec, there are a few things that might go wrong with these passive components. The first thing is the coupling between the waveguide and vernier ring if there is exceptionally low optical power received (have seen some losses in the IR camera). Another thing that losses through the loop mirror because of waveguide bending and the used taper for connecting different materials waveguides.

5. Conclusion and Future Work

In conclusion, for exploring the laser sources for photoacoustic spectroscopy, we have worked with SiN laser and aSi laser devices. For the optical characterization of these lasers, followed cold cavity measurement of passive cavities, micro-transfer printing for adding SOA-based light source, wafer dicing, chip cleaning, electronic characterization, wire bonding, and chip packaging. Although many working SiN and aSi laser devices were not giving lasers, but few of them gave lasing and delivered almost -20 dBm (10 μW) sufficient power for the absorption. For the large wavelength tunability of the laser certainly will benefit to detection of several molecules from a single laser. We have seen the wide approximately 70 nm wavelength tuning range via single vernier sweeping. We have also seen the tuning Sagnac has negligible wavelength tuning and doesn't have much effect on output power. Although for laser modulation, we haven't many lasers to perform this experiment, but based on the result of the performed modulation on the DBR lasers it offers more than 500 KHz modulation frequencies for large signals and more than 20MHz bandwidth for the small signal Which allows sensitive photoacoustic measurement. We have seen the sine wave modulation has less waveform distortion than the square wave modulation for these lasers. Finally, I can conclude that these lasers can be used for sensitive photoacoustic spectroscopy experiments.

At this point, there are several ways to proceed with this work in the future. The first step is to perform photoacoustic spectroscopy experiments with these lasers and check their sensitivity and performance. Also, each tunable laser die is compatible to deliver a combined four different wavelengths in output at the same time so in the future all the cavities should filled with SOA to get very large tunability from 1400nm to 1700nm which is almost 300nm tuning. With the alone single laser, I have demonstrated the nearly 70nm tunability, so it is possible to get nearly 300nm wide tuning with a single laser die. Most importantly future batches need to improve the μTP process for SOA printing so major devices can work and improve coupling issues from SOA to waveguide. For the increasing laser output power SOA can be improved and also, there will be possible improvements in the design side, especially the loop mirror and taper which are used to connect different waveguides and with certain improvements possibly to use in PAS-based sensing devices.

Bibliography

1) Thomson, David et al., Roadmap on silicon photonics. Journal of Optics. (2016).

2) Yang, J., Tang, M., Chen, S. *et al.* From past to future: on-chip laser sources for photonic integrated circuits. *Light Sci Appl* 12, 16 (2023).

3) Baets, Roel et al., Spectroscopy-on-chip applications of silicon photonics. Proceedings of SPIE - The International Society for Optical Engineering (2013).

4) Besson, Jean-Philippe et al., multi-gas sensing based on photoacoustic spectroscopy using tunable laser diodes. Spectrochimica acta. Part A, Molecular and biomolecular spectroscopy. (2004)

5) Angelo Sampaolo, et al., Quartz-enhanced photoacoustic spectroscopy for multi-gas detection: A review, Analytica Chimica Acta, Volume 1202, (2022).

6) I. E. Gordon, *et al.*, "The HITRAN2020 molecular spectroscopic database", *J. Quant. Spectrosc. Radiat. Transfer* 277, 107949 (2022)

7) S. Dhoore, G. Roelkens and G. Morthier, "Fast Wavelength-Tunable Lasers on Silicon," IEEE Journal of Selected Topics in Quantum Electronics, vol. 25, no. 6, pp. 1-8, (2015).

8) R. Wang et al., "Widely Tunable III–V/Silicon Lasers for Spectroscopy in the Short-Wave Infrared," in IEEE Journal of Selected Topics in Quantum Electronics, vol. 25, no. 6, pp. 1-12, Nov.-Dec. 2019

9) Billet, Maximilien, et al. "Heterogeneous tunable III-V-on-silicon-nitride mode-locked laser emitting wide optical spectra." *Photonics Research* 12.3 (2024): A21-A27.

10) Bell, A.G. (1880) On the production and reproduction of sound by light: The photophone. Am. J. Sci., 20: 305–324.

11) Kerr, E.L. and Atwood, J.G. (1968) The laser illuminated absorptivity spectrophone: A method for measurement of weak absorptivity in gases at laser wavelengths. Appl. Optic., 7: 915– 921.

12) Li, Jingsong & Chen, Weidong & Yu, Benli. (2011). Recent Progress on Infrared Photoacoustic Spectroscopy Techniques. Applied Spectroscopy Reviews. 46. 440-471.

13) Fathy, Alaa, et al. "Direct absorption and photoacoustic spectroscopy for gas sensing and analysis: a critical review." *Laser & Photonics Reviews* 16.8 (2022)

14) Walden, P. et al., Micromachined Hotplate Platform for the Investigation of Ink-Jet Printed, Functionalized Metal Oxide Nanoparticles. J. Microelectromech. Syst. 2015.

15) Palzer, Stefan. (2020). Photoacoustic-Based Gas Sensing: A Review. Sensors. 20. 2745. 10.3390/s20092745.

16) Haisch, Christoph. (2011). Photoacoustic spectroscopy for analytical measurements. Measurement Science and Technology. 23. 012001.

17) Faist, J et al. "Quantum cascade laser." *Science (New York, N.Y.)* vol. 264,5158 (1994): 553-6.

18) Sigrist, M., Bartlome, R., Marinov, D. *et al.* Trace gas monitoring with infrared laser-based detection schemes. *Appl. Phys. B* 90, 289–300 (2008).

19) L. A. Coldren, et al, "Tunable semiconductor lasers: a tutorial," IEEE J. Lightw. Technol., vol. 39, pp. 193–202, January 2004.

20) R. Baets, et al. "4 Ways to Put Lasers on Silicon: You Can Make Many Things with Silicon Photonics, But a Laser is not One of Them," in IEEE Spectrum, vol. 60, no. 5, pp. 32-37, May 2023.

21) E. Menard, et al., A printable form of silicon for high-performance thin film transistors on plastic substrates. Applied Physics Letters, 84:5398 – 5400, July (2004).

22) Zhang, Jing. III-V-on-Si Transceivers Based on Micro-Transfer-Printing. Ghent University. Faculty of Engineering and Architecture, 2021.

23) Tang, H, et al. A Review of High-Power Semiconductor Optical Amplifiers in the 1550 nm Band. Sensors 2023, 23, 7326.

24) Aneesh Sobhanan, et al., "Semiconductor optical amplifiers: recent advances and applications," Adv. Opt. Photon. 14, 571-651 (2022)

25) G. Roelkens *et al.*, "Micro-Transfer Printing for Heterogeneous Si Photonic Integrated Circuits," in *IEEE Journal of Selected Topics in Quantum Electronics*, vol. 29, no. 3 , pp. 1-14, May-June 2023

26) Soltanian, Emadreza et al., Micro-transfer-printed narrow-linewidth III-V-on-Si double laser structure with a combined 110 nm tuning range. Optics Express. (2022).

27) Zhang, Jing, et al. "Transfer-Printing-Based Integration of a III-V-on-Silicon Distributed Feedback Laser." OPTICS EXPRESS, vol. 26, no. 7, (2018)

28) B. Haq, et al., Micro-Transfer-Printed III-V-on-Silicon C-Band Semiconductor Optical Amplifiers. Laser & Photonics Reviews 2020, 14, 1900364.

29) Selvaraja, Shankar Kumar & Dumon, Pieter & Bagaerts, W & Thourhout, D & Baets, Roel. (2009). Amorphous silicon: for advanced photonic integrated circuits.

30) Agarwal, A.M., Michel, J. (2019). Amorphous Silicon in Microphotonics. In: Musgraves, J.D., Hu, J., Calvez, L. (eds) Springer Handbook of Glass. Springer Handbooks. Springer, Cham.

31) Uvin, Sarah & Keyvaninia, Shahram & Thourhout, Dries & Roelkens, Gunther. (2016). A novel approach of integrating III-V on the silicon nitride platform.

32) Op de Beeck, Camiel et al., (2020). Heterogeneous III-V on silicon nitride amplifiers and lasers via microtransfer printing. Optica. 7. 10.1364/OPTICA.382989.

33) Wim, Bogaerts, et al., Silicon microring resonators. Laser & Photonics Reviews, (2012)

34) Wang R, et al., Compact GaSb/silicon-on-insulator 2.0x μm widely tunable external cavity lasers. Opt Express; Dec 2016.

35) Liu, S., Feng, J., Tian, Y. et al. Thermo-optic phase shifters based on silicon-on-insulator platform: state-of-the-art and a review. Front. Optoelectron. 15, 9 (2022)

36) Song, Junfeng. (2012). Silicon Nanowire-Based Thermo-Optical TunableReflector. International Journal of Information and Electronics Engineering. 10.7763/IJIEE.2012.V2.223.

37) A. R. Alves Júnior, "Building blocks and subcircuits for programmable silicon photonic circuits," 2019.

38) Hamed Arianfard, Saulius Juodkazis, David J. Moss, Jiayang Wu; Sagnac interference in integrated photonics. Appl. Phys. Rev. 1 March 2023; 10 (1): 011309.

Appendix

PCB Designs:

The earlier design work focused on making a single PCB that can be used for all three lasers. However, after spending some time creating a single PCB design realized that it is more convenient to design separate individual PCBs for each one instead of a single design because the DFB laser bond pads are on both sides of the chips which is quite tricky to design and an obstacle for making a single design. So finally, I have decided to proceed with three different PCB designs for individual lasers.

The summary of the first PCB design for the aSi laser was already discussed in the main part above. Here I will discuss some design methods followed, To reach the final PCB, the first step is to make symbols and connections in the schematic editor. As from the aSi laser design, the two rows are named top (the first row) and bottom (the second row) and both have 23 pads means a total of 46 pads which are named from 0 to 22, Let's call them top_0 to Top_22 and bottom_0 to bottom_22, respectively. To make symbols it is necessary to understand the pad pin connections to the lasers because some pins are commonly grounded, and some are not even connected to any pads. following started to create a symbol in the schematic editor in KiCad and used many symbols that were pre-available. Out of 46 pads, only 40 pins are connected, and 4 pins are commonly grounded so chose to use connector 02x18_Odd_Even for a total 36 number of pads. But there are 10 extra pins connector 02x05_Odd_Even was added for future uses. For both connectors, the Surface-Mounted (SMD) pin header footprint was pre-available. The SMD footprint is very helpful in getting completely isolated from the backside of the PCB compared to the Through-hole pin header footprints. The general SMD footprint and the schematic editor are shown in *Figure 33*.

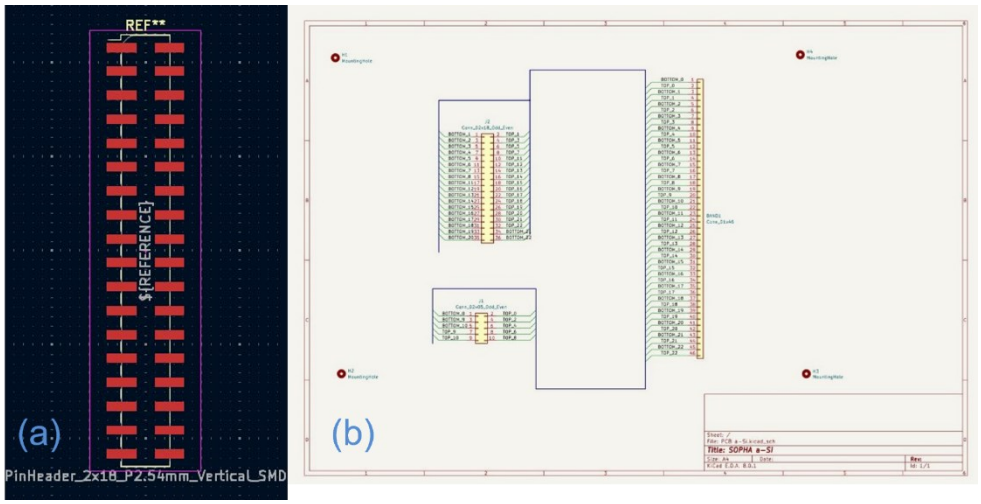

Figure 33: (a) SMD footprint of Pinheader_02x18, (b) Schematic Editor image of the design of aSi laser

The footprint design should be a perfect copy of the real one, which means the same area, size, and pitch distance of the bond pads as on the chips. The footprint is the physical representation of the real dimensions and arrangements of the pads. *Figure*

33(b) shows the Schematic editor image drawing of the aSi laser where J1 and J2 are the two connectors that relate to the BAND1 connector via a blue bus with green wires.

Now switching to the PCB Editor mode, first imported the schematic footprint design on the editor view and rearranged it with the requirement. The heatsink region was created with pin-through holes where the laser chip is going to be placed. The BAND1 SMD footprint is placed very close to this heatsink region for wire bonding purposes. The most important thing is to fix the location of mounting skew holes in the PCB design based on the metallic plate that will be used for this PCB to be placed on setup, so 4 holes were placed 56mm horizontally and 25mm vertically 4.3mm M4 on the pad. After properly placing all the components the final most crucial and tricky part of routing of wire. Here the two-layer PCB was designed by adding vias holes to reach one layer to another layer of PCB during routing. The maximum thickness used for the wire is 0.2mm and near the pads it is 0.1mm only. The finishing was done by adding another silkscreen layer that can be placed with the pin's names and numbers on the front and back sides of the PCB. The final PCB design for the aSi laser is shown in *Figure 34*.

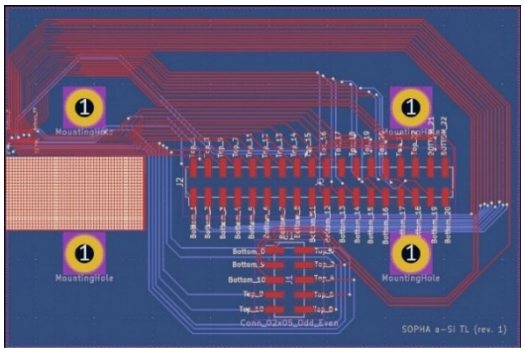

Figure 34: Final designed PCB editor view for aSi laser

The same method and ideology have been used to design the other two SiN and DFB lasers. Similar steps I have followed from the schematic drawing to assigned footprints and PCB editing. The similar way the heatsink is designed and placed at the edge of the PCB satisfies SiN laser design and the third design for the bank of DBR lasers.

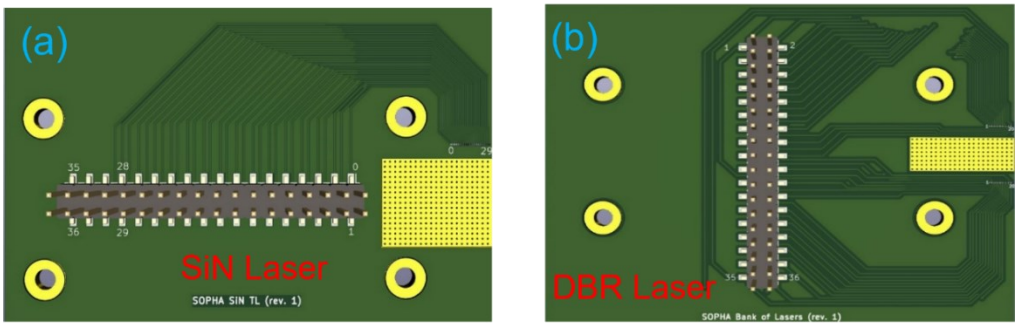

Figure 35: 3D view of the PCB Design (a) for SiN laser (b) for DBR Bank of Lasers

After designing the final PCB's 3D view for the SiN laser and bank of laser is shown in *Figure 35* Can see the routing, the screw holes, and the heatsink in yellow.

DBR Laser Cold Cavity Results

In the main part discussed the cold cavity result of Tunable SiN and aSi lasers, while here we see the result of the DBR laser. *Figure 36* shows the cold cavity result of the DBR bank of lasers.

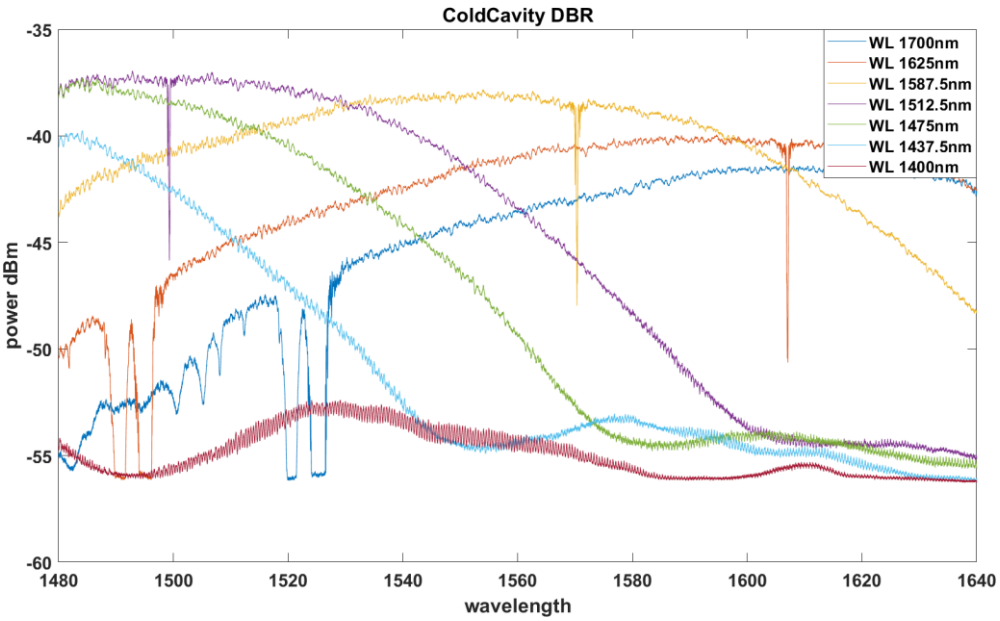

Figure 36 Cold cavity analysis of DBR Bank of lasers for different wavelengths

As from the DBR bank of laser plots, we can see each wavelength has different power and shows lasing conditions. It is noticed that these results show the blue shifts for all of the wavelengths. The reason behind this shift is not confirmed but most likely the three reasons making SOA sources, μTP process, or fabrication errors.